New Age and Geochemical Data from the Southern Colville and Kermadec Ridges, SW Pacific: Insights into the recent geological history and petrogenesis of the Proto-Kermadec (Vitiaz) Arc

C. Timm[1*2], C.E.J. de Ronde[1], K. Hoernle[2,3], B. Cousens[4], J-A. Wartho[2], F. Caratori Tontini[1], R. Wysoczanski[5], F. Hauff[2] and M. Handler[6]

[1]*GNS Science, PO Box 30-368, Lower Hutt, New Zealand*
[2]*GEOMAR, Helmholtz Center for Ocean Research Kiel, Wischhofstrasse 1-3, 24148 Kiel, Germany*
[3]*Institut für Geowissenschaften, Christian-Albrechts-Universität zu Kiel, Ludewig-Meyn-Strasse 10, 24118 Kiel, Germany*
[4]*Department of Earth Sciences, Carleton University, 1125 Colonel By Drive, Ottawa ON. K1S5B6 Canada*
[5]*National Institute of Water and Atmospheric Research, PO Box 14-901, Wellington, New Zealand*
[6]*School of Geography, Environment and Earth Sciences, Victoria University of Wellington, PO Box 600, Wellington 6140, New Zealand*

* corresponding author: c.timm@gns.cri.nz

Abstract

The intra-oceanic Kermadec arc system extends ~1300 km between New Zealand and Fiji and comprises at least 30 arc front volcanoes, the Havre Trough back-arc and the remnant Colville and Kermadec Ridges. To date, most research has focussed on the Kermadec arc front volcanoes leaving the Colville and Kermadec Ridges virtually unexplored. Here, we present seven $^{40}Ar/^{39}Ar$ ages together with a comprehensive major and trace element and Sr-, Nd-, and Pb-isotope dataset from the Colville and Kermadec Ridges to better understand the evolution, petrogenesis and splitting of the former proto-Kermadec (Vitiaz) Arc to form these two remnant arc ridges. Our $^{40}Ar/^{39}Ar$ ages range from ~7.5-2.6 Ma, which suggests that arc volcanism at the Colville Ridge occurred continuously and longer than previously thought. Recovered Colville and Kermadec Ridge lavas range from mafic picro-basalts (MgO = ~8 wt.%) to dacites. The lavas have arc-type normalized incompatible element patterns and Sr and Pb isotopic compositions intermediate between Pacific MORB and subducted lithosphere (including sediments, altered oceanic crust and serpentinised uppermost mantle). Geochemically diverse lavas, including ocean island basalt-like and potassic lavas with high Ce/Yb, Th/Zr, intermediate $^{206}Pb/^{204}Pb$ and low $^{143}Nd/^{144}Nd$ ratios were recovered from the Oligocene South Fiji Basin (and Eocene Three Kings Ridge) located west of the Colville Ridge. If largely trench-perpendicular mantle flow was

operating during the Miocene, this geochemical heterogeneity was likely preserved in the Colville and Kermadec sub arc mantle. The Colville and Kermadec Ridge data therefore highlight the complex interplay between pre-existing mantle heterogeneities and material fluxes from the subducting Pacific Plate. The new data allow us to present a holistic (yet simplified) picture of the tectonic evolution of the late Vitiaz Arc and northern Zealandia since the Miocene and how this tectonism influences volcanic activity along the Kermadec arc at the present.

1. Introduction

Volcanic arcs on Earth span ~22,000 km, predominantly manifested as the 'Ring of Fire', marking convergent Pacific Plate margins (e.g., de Ronde et al., 2001; Leat and Larter, 2003). Of those ~22,000 km of arc volcanoes, ~6900 km are largely submarine (intraoceanic) and are commonly highly active volcanically and hydrothermally. These volcanoes are therefore focus sites for element transfer from the earth's mantle into the hydrosphere and atmosphere. It is well known that magmatism beneath arc volcanoes is a consequence of hydrous mineral breakdown and related dehydration of the subducting lithospheric plate as pressure and temperature increase with increasing depth of subduction (e.g., McCulloch and Gamble, 1991; Brenan et al., 1995). As a consequence of million-year-long exposure to seawater and consequent hydration of the descending plate, the sediments, oceanic crust and the uppermost lithospheric mantle can store large amounts of water (e.g., Fisher et al., 2003). When the descending slab dehydrates, aqueous fluids and melts migrate into the overlying mantle wedge and lower the peridotite ± pyroxenite solidus below the ambient upper mantle temperature. This leads to partial melting in the mantle wedge. The resulting melts then percolate upwards to pool at density barriers such as the Moho or within the crust to ultimately form new arc crust and arc front volcanoes.

The Kermadec arc system north of New Zealand is one of the prime sites to study processes related to submarine arc volcanism. This largely submarine intraoceanic arc system comprises, from west to east: The remnant Colville Ridge, the active Havre Trough (back arc), the active Kermadec arc front (volcanoes) and remnant Kermadec Ridge (Fig. 1).

Research to date has largely focused on the exploration of volcanically or hydrothermally active arc front volcanoes (e.g., Gamble et al., 1993; Haase et al., 2002; de Ronde et al., 2001; de Ronde et al., 2007; Timm et al., 2014), leaving the inactive parts of the system (comprising ~75% of the areal extent) underexplored. Therefore, little is known about the geology or lava chemistry of the Colville and Kermadec Ridges that border the active Kermadec arc system to the west and east, respectively. This contribution is part of a series of three publications about the Colville Ridge, and presents seven $^{40}Ar/^{39}Ar$ ages, and a comprehensive major and trace element and Sr-Nd-Pb-isotope dataset on samples recovered from the southern Colville and southern Kermadec Ridges.

2. Geological Background

2.1 The Kermadec arc system

The mainly submarine Tonga-Kermadec arc system, extending ~2,500 km from north of New Zealand toward Fiji and Samoa, is one of the most hydrothermally and volcanically active intra-oceanic arcs on Earth (24 of the 33 arc front volcanoes are hydrothermally active). Driven by westward subduction of the Pacific Plate, convergence rates decrease from ~24 cm/yr. at the northern Tonga Trench down to ~5 cm/yr. at the southern Kermadec Trench (e.g., DeMets et al., 1994). The decrease in plate convergence rates is accompanied by a decrease in associated back-arc opening rates from ~15 cm/yr. in the northern Lau Basin to ≤ 1cm/yr. in the southern Havre Trough (e.g., Schellart and Spakman, 2012). Crustal thickness, as determined from wide-angle refraction seismic studies, ranges from ~13 km beneath the Colville Ridge to 15 km beneath the Kermadec Ridge at ~29˚S. Between the two ridges, crustal thickness decreases to ~11 km at ~33˚S. Further south the crustal thickness beneath the Kermadec Ridge increases to ~17.5 km just north of East Cape, New Zealand, at ~37˚S (e.g., Bassett et al., 2010; Bassett et al., 2016). The angle of the subducting Pacific Plate shallows from an average of ~20˚ at 33˚S to ~17˚ at ~34˚S in the uppermost 20 km below the seafloor (e.g., Bassett et al., 2010; Scherwath et al., 2010; Bassett et al., 2016). Below ~40 km depth, the angle of the subducting Pacific Plate changes to ≥ 45˚ (e.g., van der Hilst, 1995).

2.2 Structure of the Colville and Kermadec Ridges

Colville Ridge

The Colville Ridge forms the southern ~1,300 km segment of the Lau-Colville Ridge that bounds the west-side of the Lau Basin-Havre Trough back-arc basin system (Fig. 1). High-resolution bathymetric and geophysical mapping, together with rock dredging undertaken in 2013 and 2015 during the Colville I and Colville II surveys with R/V *Tangaroa* and 2017 during the SO255 Vitiaz cruise, confirm that the Colville Ridge is volcanic and reaches water depths as shallow as ~500 mbsl (meters below sea-level) on the southernmost three segments trending northeast – southwest, paralleling the Kermadec Ridge and Trench (see also Wright, 1997; Fig 2). Numerous faulted and intact volcanic edifices dot the ridge-crest and the western flank of this ridge. The Colville Ridge segments are separated by seafloor lows as deep as ~2,500 mbsl at 34˚15' S. North of this seafloor low the ridge is relatively narrow and composed of sub-parallel segments, before significantly widening and shallowing north of ~32˚S.

Prominent arc-perpendicular chains of comparably small volcanic edifices, some of which sit on shallow seafloor, cut the Colville Ridge at 35˚40'S (Rumble ridge; cf. Gamble et al., 1995; Todd et al., 2010), 34˚40'S, 33˚35'S and 33˚0'S. Segmentation of the Colville Ridge occurs where these chains intersect the Colville Ridge. Furthermore, a deeply eroded northwest-southeast elongated flat-topped guyot and ridge-like volcanic structure is located in the South Fiji Basin directly west of where the cross chains cut the Colville Ridge.

Kermadec Ridge

Bounding the Havre Trough to the east is the Kermadec Ridge, which forms the southern part of the ~1,300 km long segment of the Tonga-Kermadec Ridge. Similar to the Colville Ridge, the Kermadec Ridge is segmented and generally widens towards the north from <10 km at ~36˚S to > 25 km at ~33˚S. Wright (1997) defines five Kermadec Ridge segments between ~36˚30˚S and ~32˚S. The Kermadec Ridge, much like the Colville Ridge, is asymmetrical with a steep west-facing (up to ~1000 m high) fault scarp

bordering the eastern side of the Havre Trough and more gentle sloping eastern flank, forming the Kermadec forearc.

2.3 Distribution of regional volcanism at the northern Lau and Tonga Ridges since the Eocene

The oldest submarine rocks recovered thus far from the Tonga arc system in the north are 51-39 Ma old arc gabbros, back-arc basin and arc-type tholeiites dredged from the Tonga forearc (e.g., Meffre et al., 2012; Falloon et al., 2014). Contemporaneous, 46-40 Ma old, arc-type basement lavas are exposed on Eua Island, along the Tonga Ridge (e.g., Duncan et al., 1985). Upper Eocene to Miocene rocks of the Yavuna Group (a ~34-25 Ma old sequence of early arc eruptives, including boninites and island arc tholeiites; e.g., Whelan et al., 1985; Gill, 1987; see also summary in Todd et al., 2012) are exposed in Fiji on Vitu Levu, at the northern end of the Lau Ridge. Between ~15 and 5 Ma, bimodal arc-type volcanism formed arc volcanoes of the Lau Volcanic Group atop the Lau Ridge (e.g., Gill et al., 1984; Hergt and Woodhead, 2007). The Lau Ridge began to split at ~6 Ma, related to the initial opening of the Lau Basin (e.g., Parson and Hawkins, 1994; Taylor et al., 1996; Zellmer and Taylor, 2001). Volcanism on the Lau Ridge recommenced at ~4.4 Ma and continued until 2.4 Ma (the Korobasanga Volcanic Group; e.g., Gill, 1976; Whelan et al., 1985; Hergt and Woodhead, 2007 and references therein), which is surprising since the opening of the Lau Basin shifted the trench further to the east. Based on dredge samples from the Tonga Ridge, Meffre et al. (2012) proposed the existence of a third Miocene (15-9 Ma) phase of volcanism, which youngs northward and westward towards the Lau Basin. Present-day volcanism is focussed in the eastern region of the Lau Basin and along the Tonga arc front.

2.4 Current knowledge of the Geological History of the Colville and Kermadec Ridges

No early to mid-Eocene volcanic or plutonic rocks have been recovered from the Colville and Kermadec Ridges or Havre Trough back arc-Kermadec arc front to date. The nearest late Eocene (37.5 Ma) to early Oligocene (31.7 Ma) arc rocks are exposed on or near the Three Kings Ridge and the

easternmost Northland Plateau (Fig. 1 and 4; Mortimer et al., 2007). The South Fiji Basin opened in the Late Oligocene – Early Miocene with contemporaneous eruption of low and high K (shoshonitic) arc-type lavas between ~25 and 19 Ma (e.g., Herzer et al., 2011). Based on these ages and rock-types, Mortimer et al. (2007) and Herzer et al (2011 and references therein) developed a tectonic model whereby the Loyalty-Three Kings Ridge once formed a single, continuous arc with the Lau-Colville Ridge (the Vitiaz arc), and the splitting of this arc allowed the South Fiji Basin to form.

Biostratigraphic data from both the Colville and Kermadec ridges indicate that sedimentation on both ridges took place at least since the early Miocene (~25 Ma), consistent with a co-joined origin of the ridges (Ballance et al., 1999). Only two published radiometric ages of 16.68 ± 0.20 Ma (2σ; $^{39}Ar/^{40}Ar$ plagioclase; Mortimer et al., 2010) and 5.4 ± 0.1 Ma (2σ; K/Ar groundmass; Adams et al., 1994) exist from two Colville lavas obtained from a single dredge haul. Similarly, a single K-Ar age of 7.84 ± 0.64 Ma exists from a Kermadec Ridge lava cobble sampled at 7,700 mbsl at ~31˚S (Fig. 1; Ballance et al., 1999).

3. Sampling and Analytical Methods

Seafloor rock samples were recovered from 14 sites along the Colville Ridge between ~36˚S and 33˚S during the Colville I (TAN1313) and Colville II (TAN1512) research cruises, and from one Kermadec Ridge site at 36˚07.9'S/178˚25.9'E during the Nirvana (TAN1213) survey, all using R/V *Tangaroa*. Additional samples from seven Kermadec Ridge sites between 35 and 32.5˚S were recovered with R/V *Sonne* during the SO255 VITIAZ expedition.

Samples for geochemical analysis were broken into sub-centimetre-sized pieces. Only fresh fragments without sawed surfaces were handpicked under a binocular for geochemical analysis. These fragments were cleaned for several hours in an ultrasonic bath in de-ionised water to remove seawater salts; this procedure was repeated at least three times until the residue solution was clear. The Colville and two TAN1213 Kermadec Ridge sample were then dried at 60˚C, crushed, pulverized in agate mills and analysed for

major and minor elements by X-ray fluorescence (XRF) and trace elements by ICP-MS at the Ontario Geoscience Laboratories (OGL) in Sudbury, Canada. The Kermadec Ridge samples collected with R/V *Sonne* were analysed for major and minor elements by XRF at the University of Hamburg and for trace elements by ICP-MS at the University of Kiel. Major and minor element XRF analyses were performed on fused glass discs using lithium metaborate as flux at both labs. Similarly, for trace element analysis, samples were digested in a mixture of nitric, hydrofluoric, perchloric and hydrochloric acid in closed vessels. Procedural details can be found in Burnham and Schweyer (2004) (OGL) and Garbe-Schoenberg et al. (1993) (University of Kiel). Relative deviations between measured standards and their reference values are within ≤ 7% (mostly ≤ 3%), except for Cs, Cu, Mo, Sb, Sn and Tl (all within ≤ 15%; see Supplementary Table 1).

Strontium, Nd, and Pb isotope analyses of samples collected with R/V *Tangaroa* were performed on a TIMS Triton at the Isotope Geochemistry and Geochronological Research Centre at Carleton University, Ottawa, using the same powders prepared for trace element analysis at OGL. Prior to dissolution, one aliquot for Sr isotope analysis was leached in hot (125˚C) 6 N HCl for five days to remove altered portions of the rock. A second aliquot for Nd and Pb isotope analysis was weakly acid-washed in warm (90˚C) 1.5 N HCl for 12 hours. Sample dissolution and chromatographic separation of Pb, Sr and Nd was based on descriptions in Cousens (1996). Total procedural blanks for Pb were < 200 picograms. Samples were loaded onto single Re filaments with H_3PO_4 and silica gel, and run at filament temperatures of 1250-1310˚C. All mass spectrometer runs were corrected for fractionation using NIST SRM981. The average ratios measured for SRM981 were $^{206}Pb/^{204}Pb$ = 16.883 ± 0.019, $^{207}Pb/^{204}Pb$ = 15.420 ± 0.017, and $^{208}Pb/^{204}Pb$ = 36.476 ± 0.046 (2 standard deviations (s.d.)), based on 50 runs between July 2015 and August 2017. The fractionation correction, based on the values of Todt et al. (1984) is +0.13%/amu. Analysis of USGS Standard BCR-2 yielded $^{206}Pb/^{204}Pb$ = 18.767, $^{207}Pb/^{204}Pb$ = 15.619, and $^{208}Pb/^{204}Pb$ = 38.742 (average of 8 runs). Total procedural blanks for Sr were < 450 picograms. Sr was loaded onto a single Ta filament with H_3PO_4 and run at filament

temperatures of 1380-1450˚C. Isotope ratios were normalized to $^{86}Sr/^{88}Sr$ = 0.1194 to correct for fractionation. Two standards were run at Carleton, NIST SRM987 ($^{87}Sr/^{86}Sr$ = 0.710250 ± 22, n=65, July 2015 - August 2017) and the Eimer and Amend (E&A) $SrCO_3$ ($^{87}Sr/^{86}Sr$ = 0.708013 ± 15, n = 10, Sept. 2010-Feb. 2014). Total procedural blanks for Nd were < 150 picograms. Samples were loaded with H_3PO_4 on one side of a Re double filament, and run at temperatures of 1780-1810˚C. Isotope ratios were normalized to $^{146}Nd/^{144}Nd$ = 0.72190. Analyses of the USGS standard BCR-2 yielded $^{143}Nd/^{144}Nd$ = 0.512644 ± 12 (n = 11). 60 runs of an in-house Nd metal standard yielded $^{143}Nd/^{144}Nd$ = 0.511828 ± 7, and 6 runs of the La Jolla standard average $^{143}Nd/^{144}Nd$ = 0.511860 ± 9 (July 2015-August 2017).
Samples collected with R/V Sonne were analysed at GEOMARs isotope facility
following the protocols of Hoernle et al. (2011). Prior to dissolution rock chips were leached in 2 N HCl at 70°C for 1-2 hours and thereafter triple rinsed in 18.2 MΩ water. Isotope analysis were carried out on a Triton-Plus TIMS operating in static multi-collection. Within run normalization for Sr and Nd is similar to Carleton University. Sample data is reported relative to $^{87}Sr/^{86}Sr$ = 0.710250 ± 8 (2 s.d.; n = 38) for SRM987 and $^{143}Nd/^{144}Nd$ = 0.511850 ± 5 (2 s.d.; n = 35) for La Jolla that were measured along with the samples. Pb mass bias correction uses the double-spike (DS) procedure of Hoernle et al. (2011). DS corrected SRM981 ratios since installation of the instrument in 2014 are $^{206}Pb/^{204}Pb$ = 16.9407 ± 18, $^{207}Pb/^{204}Pb$ = 15.4976 ± 19, and $^{208}Pb/^{204}Pb$ = 36.7200 ± 0.0046 (2 s.d., n = 112). Procedural blanks were <30pg for Pb, < 100pg for Sr and Nd.

Samples for $^{40}Ar/^{39}Ar$ analyses were crushed, dry sieved and cleaned with distilled water in an ultrasonic bath, and plagioclase separates and sample matrix were handpicked using a binocular microscope. The $^{40}Ar/^{39}Ar$ analyses were all conducted at the GEOMAR Argon Geochronology (ARGO) Laboratory. A summary of the $^{40}Ar/^{39}Ar$ results is shown in Table 2, and the complete $^{40}Ar/^{39}Ar$ dataset for the 7 samples and detailed analytical

background are presented in Supplementary File 2 and 3 and Table 2. All ages are quoted with 2σ errors, unless otherwise stated.

4. Results

4.1 Petrology and Mineralogy

The new samples of Colville and Kermadec Ridge lavas are dense to slightly vesicular. Macroscopically these lavas range from aphyric to porphyritic with up to 20 volume % (vol.%) of predominately plagioclase, clinopyroxene, olivine ± orthopyroxene and Fe-Ti oxide phenocrysts. The less phyric lavas are slightly vesicular (≤ 2 mm diameter) and contain a microcrystalline groundmass consisting of small (<1 mm) plagioclase ± clinopyroxene, plus trace olivine. The groundmass of these lavas is mainly crystalline with minor devitrified interstitial glass. The more porphyritic lavas are variably vesicular and contain more plagioclase than pyroxene, with crystals up to 5 mm across. Less abundant, but still forming mm-sized crystals, are olivine (≤ 2 vol.%) and Fe-Ti oxides. In addition, both plagioclase-pyroxene (± olivine and Fe-Ti oxide) and less common olivine-pyroxene glomerocrysts of up to 8 mm across are the major constituents in the porphyritic lavas.

4.2 Age determinations

New plagioclase $^{40}Ar/^{39}Ar$ ages for three Colville Ridge and one Kermadec Ridge, plus three groundmass Kermadec Ridge lavas are presented in Table 2 and Figure 3. The oldest age of 6.9 ± 1.6 Ma comes from a lava dredged from a small split volcanic edifice at the southernmost Colville Ridge (~35.6˚S; TAN1313 DR11-1). This sample yields a plateau age of 7.5 ± 2.0 Ma (Mean Square Weighted Deviation (MSWD) = 1.57, probability (P) = 14%; 70.9% ^{39}Ar), and low $^{36}Ar/^{37}Ar$ Alteration Index (AI) values for the majority of the medium- and high-temperature steps indicating the degassing of fresh plagioclase (Table 2; Supplementary File 3). However, an inverse isochron plot of the plateau steps shows an initial $^{40}Ar/^{36}Ar$ ($(^{40}Ar/^{36}Ar)_i$) value of 303.3 ± 6.3, which is > 295.5 (the atmospheric air $^{40}Ar/^{36}Ar$ ratio), thus

indicating the presence of excess ^{40}Ar. Therefore, we use the inverse isochron age of 6.9 ± 1.6 Ma (MSWD = 0.77, P = 60, Spreading Factor (SF) = 85.1%). The large step errors (Supplementary File 3) are due to the very low K content (<0.02 wt.% K) of this sample, which is reflected in the larger errors associated with the plateau and inverse isochron ages. A similar K/Ar age of 7.84 ± 0.69 Ma from the Kermadec Ridge at ~30.5˚S (Ballance et al., 1999) suggests that largely contemporaneous volcanism occurred on the proto Kermadec Arc (represented by combined Colville and Kermadec Ridges at that time).

Plagioclase from two Colville Ridge lavas (TAN 1512 DR16-1 and 19-2; Fig. 2 and 3) recovered from the upper ridge flank at ~33.7˚S yield significantly younger $^{40}Ar/^{39}Ar$ plateau ages of 3.80 ± 0.33 Ma (MSWD = 1.57, P = 17%, 66.1 % ^{39}Ar) and 2.63 ± 0.39 Ma (MSWD = 1.21, P = 25%, 100 % ^{39}Ar), respectively. The $^{36}Ar/^{37}Ar$ AI values indicate that these two plagioclase samples are altered, although the medium- and high-temperature steps have lower (fresher) values than the low-temperature steps (Supplementary File). Inverse isochron plots of the plateau steps of these two samples yield inverse isochron ages within 2σ errors of the plateau ages and $(^{40}Ar/^{36}Ar)_i$ values within error of the $^{40}Ar/^{36}Ar$ air ratio (Table 2; Supplementary File 3), giving us confidence in these plateau ages.

The two TAN 1512 Colville Ridge plagioclase $^{40}Ar/^{39}Ar$ ages are similar to a new $^{40}Ar/^{39}Ar$ plagioclase high-temperature plateau age of 3.40 ± 0.24 Ma (MSWD = 1.04, P = 40%, 63.5% ^{39}Ar) from a southernmost Kermadec Ridge lava dredged at ~36.4˚S (TAN1213 DR64-1). This plagioclase sample also preserves a younger low-temperature plateau age of 3.06 ± 0.25 Ma (MSWD = 0.79, P = 40%, 63.5 % ^{39}Ar). The $^{36}Ar/^{37}Ar$ AI values indicate that this plagioclase sample is altered, but the high-temperature plateau age originates from fresher material, thus this age is preferred to the younger low-temperature plateau age. Both plateau ages yield inverse isochron ages identical to the plateau ages and show $(^{40}Ar/^{36}Ar)_i$ values within 2σ errors of the atmospheric $^{40}Ar/^{36}Ar$ ratio (Table 2). Three Kermadec Ridge groundmass $^{40}Ar/^{39}Ar$ ages from Sonne cruise 255 yield similar plateau and pseudo-plateau ages of 4.44 ± 0.36 and 4.04 ± 1.23 Ma (2 splits for sample DR30-4,

with a combined weighted mean age of 4.41 ± 0.35 Ma), 4.6 ± 1.6 Ma (DR139-2) and 4.8 ± 1.2 Ma (DR179-5; Table 2; Figure 3). Unfortunately, these samples had high Cl concentrations (resulting in suppression in some initial Ar isotope measurement cycles), were variably altered, some had low K contents, and they were overirradiated (older ages were expected, resulting in low $^{40}Ar^*/^{39}Ar$ ratios of < 3), which resulted in large step errors and weighted mean ages. However, despite these issues, the 3 groundmass samples did yield plateau/pseudo-plateau ages that originated from fresh/slightly altered material (i.e., shown by the low $^{36}Ar/^{39}Ar$ AI ratios), which overlap with the inverse isochron ages, and show $(^{40}Ar/^{36}Ar)_i$ values within 2σ errors of the atmospheric $^{40}Ar/^{36}Ar$ ratio (Table 2).

These seven new $^{40}Ar/^{39}Ar$ plagioclase and groundmass ages, together with a previously published K/Ar and a previously published $^{40}Ar/^{39}Ar$ age (Adams et al., 1994; Balance et al., 1999), confirm that contemporaneous volcanism occurred on the Colville and Kermadec Ridges between ~7-8 Ma and ~3-5 Ma (cf. Figs. 2 - 4).

4.3 Major and trace element compositions

As is common for pre-Quaternary seafloor rocks, traces of alteration are invariably present. Even after careful sample preparation, four of the Colville and Kermadec Ridge lavas show high loss of ignition (LOI) values of (> 3.5 wt.%) and six have P_2O_5, (>0.5 wt.%) in addition to high U, Cs and Li contents suggesting that seawater alteration may have affected some of the incompatible LILE contents. No systematic correlation, however, exists between LOI and either of the alkalies (Na_2O or K_2O). The alkalies however form a coherent positive trend with wt. SiO_2, indicating that they have survived major seawater alteration. Therefore, we use the alkali-based classification scheme of LeMaitre et al. (2002) and Gill (1981). Following the rock classification of LeMaitre et al. (2002), the compositions of the Colville and Kermadec Ridge lavas range from picro-basalt through basalt, basaltic andesite to dacite, (45-66 wt.% SiO_2 and 7.6-1.2 wt.% MgO; Fig.5a). Except for one lava from the Colville Ridge and two from a seamount west of the Colville Ridge, all lavas plot within the medium-K calc-alkaline series after Gill

(1981) (Fig. 5b) and the ppm Th-Co variance (not shown) defined by Hastie et al. (2007). The major element oxides of the Colville and Kermadec lavas, including Al_2O_3, (and K_2O and to a lesser extent Na_2O), plot at the higher end of the spectrum defined by the Kermadec arc front and Havre Trough lavas (Figs. 6a-6g). Two lavas from a seamount ~2 km west of the Colville Ridge (in the South Fiji Basin; TAN1512 DR11-1 and 11-2) have low SiO_2, total FeO (FeO^t) and MgO, but high TiO_2 and Al_2O_3 contents suggesting a different origin for these lavas.

On multi-element diagrams (normalised to normal mid-ocean ridge basalt; NMORB; after Sun and McDonough,1989), the Colville and Kermadec Ridge lava minor and trace element patterns resemble those typical of island arc basalts, with high contents of large ion lithophile elements (LILE; e.g., Ba, Pb, Sr, K) and negative Nb and Ta anomalies (Fig. 7a). Although LILE contents of the Kermadec arc front and Colville and Kermadec Ridge lavas overlap, the two South Fiji basin seamount lava samples have higher contents of Th and the high field strength elements (HFSE; i.e., Nb, Ta, Zr, and Hf, and rare earth elements (REE)). The Colville and Kermadec Ridge lavas have higher more to less incompatible element ratios (e.g., Th/Zr, Ce/Yb, $(La/Sm)_N$, Sm/Yb, Nb/Y and Nb/Yb ratios; Figs. 7-10) than lavas from the Havre Trough and Kermadec arc front volcanoes. The two lavas from the South Fiji Basin seamount west of the Colville Ridge have distinct major and trace element compositions with high Nb (30 ppm) and Ta (1.8 ppm) contents, and moderately high Y, Zr, Hf and REE concentrations at a given SiO_2 content, when compared to the other Colville and Kermadec Ridge lavas (e.g., Fig. 7b and 8-10).

4.4 Sr-, Nd-, and Pb-isotopic compositions

A subset of Colville (n = 19) and Kermadec Ridge lavas (n = 17) were analysed for their Sr-, Nd-, and Pb-isotopic compositions. Sr, Nd and Pb isotopic compositions of the Colville Ridge lavas ($^{87}Sr/^{86}Sr$ = 0.70396 to 0.70449; $^{143}Nd/^{144}Nd$ = 0.51289 to 0.51298; $^{206}Pb/^{204}Pb$ = 18.62 to 18.76; $^{207}Pb/^{204}Pb$ = 15.55 to 15.62 and $^{208}Pb/^{204}Pb$ = 38.47 to 38.71) overlap with those from the Kermadec Ridge ($^{87}Sr/^{86}Sr$ = 0.70395 to 0.70439; $^{143}Nd/^{144}Nd$ = 0.51293 to 0.51301; $^{206}Pb/^{204}Pb$ = 18.55 to 18.83; $^{207}Pb/^{204}Pb$ = 15.56 to

15.63 and $^{208}Pb/^{204}Pb$ = 38.55 to 38.74; Figs. 11a-11d). Although there is nearly complete overlap between data from the Kermadec and Colville Ridges, except that Colville lavas extend to slightly less radiogenic Nd isotopic ratios and Kermadec lavas to slightly more radiogenic $^{206}Pb/^{204}Pb$ isotope ratios. Compared to the Quaternary Kermadec volcanic front and Havre Trough back arc lavas, most Kermadec and Colville Ridge samples are shifted to lower $^{206}Pb/^{204}Pb$ at a given $^{87}Sr/^{86}Sr$, $^{143}Nd/^{144}Nd$ and $^{208}Pb/^{204}Pb$ for the modern arc and back arc (Fig. 11). Four Kermadec Ridge lavas have more radiogenic Pb isotopic composition similar to that of the Quaternary Kermadec volcanic front lavas. The two South Fiji Basin seamount lavas have more radiogenic Pb (e.g., $^{206}Pb/^{204}Pb$ = 19.0), radiogenic $^{143}Nd/^{144}Nd$ (0.51299-0.51301) and less radiogenic Sr isotopic compositions (0.7030-0.7031) than the Colville lavas, plotting in the field defined by other South Fiji Basin lavas (Fig. 11).

5. Discussion

5.1 Temporal evolution of the Colville and Kermadec Ridges: Filling the age gap

Combining one published $^{40}Ar/^{39}Ar$ age (16.68 ± 0.20 Ma; Mortimer et al., 2010), two published K-Ar ages (5.4 ± 0.1 Ma, Adams et al., 1994; 7.84 ± 0.69 Ma, Balance et al., 1999) and our seven new $^{40}Ar/^{39}Ar$ ages of 6.9 ± 1.4 Ma (isochron age) and 4.80 ± 1.6 - 2.63 ± 0.23 Ma (Table 2; Fig. 3) indicates that volcanism on the Colville and Kermadec Ridges has been active for at least ~13 Ma from the mid Miocene to late Pliocene (16.7 to 2.6 Ma). The similar ages determined on both ridges of ~7-8 and ~3-5 Ma also demonstrate that volcanism on both ridges was contemporaneous and that the Colville Ridge volcanism continued for ~2.8 Myrs longer than previously believed based on the youngest published Colville Ridge lava age of 5.4 Ma. Four of the seven new ages range from 4.8±1.2 to 3.8±0.33 suggesting that volcanism may have been particularly active during this time. This age range is similar to the age of ~5 Ma proposed for the initial opening of the Havre Trough, based on the extrapolation of geodetic data from onshore New Zealand (Wright et al., 1993). This raises the question whether the arc

splitting occurred rather at ~4 or even later, at least 1 Ma later than previously thought. There is independent evidence that a sequence of processes occurred between ~7 and 5 Ma onshore and to the north. Published rock and biostratigraphic ages together with migration of arc volcanism suggests acceleration of eastward arc migration from ~4-18 mm/yr. starting between ~7 and 5 Ma (e.g., Rowan and Roberts, 2008; Seebeck et al., 2013). Between 5 and 4 Ma arc volcanism on the North Island, New Zealand, switched from the southern Coromandel Volcanic Zone - the onshore extension of the Colville Ridge - to lower volume arc volcanism associated with crustal extension at the western central volcanic region (e.g., Adams et al., 1994; Briggs et al., 2003; Carter et al., 2003). The Colville $^{40}Ar/^{39}Ar$ age of 6.9 ± 1.4 Ma falls in a phase of intense onshore rhyolitic volcanism (Whitianga Group) and subordinate eruption of andesites in the central Coromandel Peninsula (e.g., Booden et al., 2012). The younger ages of 4.80-3.80 Ma are contemporaneous with crustal extension at ~4 Ma onshore. The two younger ages of 3.40 ± 0.24 and 2.63 ± 0.23 Ma post-date Coromandel arc volcanism and possibly relate to ongoing eastward migration of the Kermadec Trench and associated back-arc extension (re-) opening pathways for magmas to ascend to the surface. Given the location of these lavas on the upper Colville and Kermadec ridge flanks, the melts are likely to have ascended through pre-existing weak zones, such as crustal-scale faults bordering the Havre Trough to the east and west (e.g., Wright, 1997).

To the north, initial crustal stretching between the Lau and Tonga Ridges (accompanied by arc-type intrusions) was initiated at ~5-6 Ma (cf. ODP site 834; Parson and Hawkins, 1992), followed by southward propagating seafloor spreading at the eastern Lau spreading center between ~4-2 Ma (e.g., Taylor et al., 1996; Zellmer and Taylor, 2001). Similarly, the Lau Islands record Miocene to Pleistocene (~14 to ~0.3 Ma) magmatic activity pre- and post-dating back-arc opening (e.g., Gill, 1976; Whelan et al., 1985). Pre-dating back-arc opening are the ~14 - 5.4 Ma old Lau Volcanics that form the Lau Island volcanic arc basement. Following ~1 Myr quiescence the arc-like Korobasanga Volcanic Group erupted between ~4.4 and 2.4 Ma, post-dating initial back-arc opening. Taken together we favour that splitting of the proto-Kermadec arc may have occurred somewhat later than previously

believed, probably around 4 Ma (or even later), contemporaneously with the onset seafloor spreading in the Lau Basin and back-arc extension onshore New Zealand. The exact timing of initial back-arc formation remains, however, unclear, because of the limited age constraint from the western Havre Trough where the first post-splitting seafloor formed.

Further sampling of the western slope of the Kermadec Ridge, between 31˚07'S and 32˚20'S recovered younger basalts ranging from 0.08 ± 0.03 to 2.0 ± 0.3 Ma (Ballance et al., 1999). In addition, exposed *in situ* volcanic rocks in the central Havre Trough yield young ages of ≤ 2 Ma, and thus are related to back arc extension (e.g., Ballance et al., 1999; Mortimer et al., 2009; Zohrab, 2017). The new $^{40}Ar/^{39}Ar$ ages presented in this study therefore fill the age gap between ~5 and ~2 Ma and demonstrate that volcanism has occurred more or less continuously to the present. Continuous arc-type volcanic activity since at least ~25 Ma also took place on the North Island, New Zealand (e.g., Adams et al., 1994; Wilson et al., 1995; Heyward et al., 2001; Carter et al., 2003; Briggs et al., 2005; Booden et al., 2012; Fig. 4). Our new combined with published data suggest that contemporaneous volcanism may have occurred continuously from the northern Lau-Tonga Ridges to the North Island of New Zealand since possibly mid-Miocene times.

5.2 Do the Colville and Kermadec Ridge lavas have a common origin?

Lavas emplaced at similar times (8-3 Ma) have been recovered from both the Colville and Kermadec Ridges. Furthermore, lavas from both ridges are petrographically similar and include aphyric and highly plagioclase-, clinopyroxene (± olivine)-phyric lavas. The Kermadec and Colville Ridge lavas have similar major element compositions except for three more evolved lavas recovered from the Kermadec Ridge. Clinopyroxene, orthopyroxene and plagioclase, and to a lesser extent olivine and Ti-Fe oxide, are the main phenocryst and groundmass phases in lavas from the ridges. Generally increasing wt.% SiO_2 (and Na_2O and K_2O) contents and broadly decreasing wt.% CaO, FeO^t and Al_2O_3 with decreasing wt.% MgO on variation diagrams is consistent with fractional crystallization of the observed phenocryst phases to explain the major element variations (Figs. 5a-5e). In addition, about half of the Colville Ridge lavas contain large amounts of phenocrysts, which

suggests that the accumulation of phenocrysts (± xenocrysts) also plays a role beneath both ridges. Plagioclase and pyroxene accumulation is supported by relatively high Sc and Al_2O_3 contents and subtle positive Eu anomalies in the porphyritic Colville Ridge samples (cf. Table 1; Eu/Eu* = 1.01-1.04), when compared to the less crystal-phyric lavas (Figs. 5-6). For crystal fractionation and accumulation to occur melts were possibly stored in magma chambers in the sub-arc crust (and possibly mantle). Some of the less crystal-phyric and aphyric lavas have low silica contents, which indicates that their formation is largely related to melting in the sub-arc mantle rather than a chemical signal derived from crystal accumulation or fractionation.

The Kermadec and Colville Ridge lavas show typical arc-type multi-element patterns (i.e., negative Nb and Ta and positive LILE anomalies compared to MORB on multi-element diagrams; Figs. 6a) that nearly completely overlap on multi-element diagrams, although a few Kermadec samples show greater incompatible-element depletion than the Colville Ridge lavas. Enrichment in fluid mobile elements (Rb, Ba, U, K, Sr, Pb, Sb, and Sn), resulting in high Ba/Th ratios, are consistent with the Kermadec and Colville sub-arc mantle having been fluxed (metasomatized) with aqueous fluids/melts, derived from the subducting Pacific Plate (sediments and or ocean crust).

Although most lavas from both Ridges (and the Kermadec arc front) have largely overlapping incompatible-element characteristics, those from the Colville Ridge tend to higher $(La/Sm)_N$, Ce/Yb, Th/Zr, Nb/Y, Nb/Yb and possibly $^{87}Sr/^{86}Sr$, but lower Ba/Th and $^{143}Nd/^{144}Nd$. These differences could be explained by a higher sediment melt component in the Colville Ridge lavas, consistent with a more rear arc setting for the Colville Ridge lavas while it was part of the proto-Kermadec (Vitiaz) arc compared with a more arc front location for the Kermadec Ridge lavas. Due to the highly fluid mobile behavior of Pb in subduction zones, sediment Pb will also be transported to the source beneath the arc front by fluids, providing a possible explanation for the almost complete overlap in Pb isotopes between Kermadec and Colville Ridges. In conclusion, the Kermadec and Colville isotopic compositions can be modelled by adding 1-3 wt.% subducted sediment to a depleted Pacific MORB type mantle wedge. Of note is that four Kermadec Ridge lavas (from stations

SO255 DR32 and TAN1213 DR64) have a similar Sr, Nd and Pb isotopic composition to the Quaternary Kermadec arc front lavas. This suggests that these lavas are derived from a similar mantle than the Kermadec arc front lavas. One of these samples gave a plagioclase $^{40}Ar/^{39}Ar$ age of 3.40 ± 0.24 Ma which is younger that other dated Kermadec Ridge lavas. This could indicate that these lavas formed post-splitting at a more trench-ward location than the remaining Kermadec Ridge lavas arguing for ridge separation prior to 3.40 ± 0.24 Ma.

In summary, the similarities between the geochemical compositions, combined with their similar emplacement ages, indicates that most lavas from the Kermadec and Colville Ridges are derived from a similar source, which is different to the parental source of the modern Kermadec arc front lavas. The stated similarities support the idea that the two ridges were joined and formed a continuous volcanic arc prior to their separation, with the Kermadec Ridge located closer to the trench (the arc front) and the Colville Ridge being located more in a rear-arc position of the Miocene arc. Therefore, we henceforth discuss the Colville and Kermadec Ridges together.

5.3 Geochemical variability of the Colville and Kermadec Ridge lavas

The Quaternary Kermadec arc front and Havre Trough back arc lavas have largely distinct isotopic compositions from the older Colville and Kermadec Ridge lavas extending to overall more radiogenic Pb and Sr but overall less radiogenic Nd isotope ratios. The composition of the Quaternary arc and back arc samples cannot be simply explained by mixing of depleted Pacific type mantle wedge with a subducted sediment component, but requires an additional component with more radiogenic Pb. Addition of a mixture of subducted sediments and HIMU-type Hikurangi seamounts, however, can explain the isotope data (Timm et al., 2014).

Based on a plate reconstruction model, Timm et al. (2014) argued that the Hikurangi Plateau has subducted beneath the proto-Kermadec arc south of ~32˚S for at least the last 10 Ma. The geochemical data from the Kermadec and Colville Ridges with dated samples as young as 2.6 Ma, however, do not support the necessity of subducting the Hikurangi Plateau and Seamounts. On the other hand, the Hikurangi Plateau basement has incompatible-element

abundances similar to enriched (E) MORB, whereas the seamounts have much higher abundances of almost all incompatible elements (except the heavy rare earth elements and Y). Strontium and Nd are up to a factor of ~15 times higher and Pb is up to a factor of ~50 times higher in the seamount compared to basement lavas (Hoernle et al., 2010). Therefore, it is possible that subduction of the plateau can only be clearly established if HIMU-type Hikurangi seamounts are present on the subducted portion of the plateau, as is the case in the Quaternary Kermadec Arc (Timm et al., 2014).

When compared to the Quaternary Kermadec Arc front lavas, the Colville and Kermadec Ridge lavas have generally higher abundances of light rare earth elements (LREE: i.e., La-Sm) and Th and lower $^{143}Nd/^{144}Nd$ values at a given wt.% SiO_2. The high field strength element (Nb, Ta, Ti, Zr, Hf) and Y contents and Nb/Y and TiO_2/Yb (and Nb/Yb) of the Quaternary Kermadec arc front and Colville-Kermadec Ridge lavas are similar and N-MORB-like, suggesting a source composition similar to N-MORB (e.g., Pearce, 2008; Fig. 10a and 10b). Although a subducted Pacific Plate sediment clearly contribute to the higher LREE and Th via sediment melts or supercritical fluids it remains unresolved whether the Colville-Kermadec Ridge sub arc mantle also was geochemically heterogeneous prior to largely fluid-derived metasomatism of the mantle wedge in the Indo-Australian Plate. Assuming corner flow, i.e. mantle flow is largely perpendicular (eastward) to the Kermadec trench (as is thought to occur beneath the Kermadec arc; Timm et al., 2013), the mantle passing beneath the Colville Ridge would have undergone less prior melt extraction (to form the South Fiji Basin back-arc lavas) than the mantle beneath the present-day Havre Trough and Kermadec arc front. Therefore, it is plausible that the mantle beneath the Colville-Kermadec Ridge was somewhat less depleted in fluid immobile elements than the mantle beneath the Havre Trough and Kermadec arc front today, accounting for the fluid immobile element and Nd isotope variations observed in the Colville and Kermadec Ridge lavas (Figs. 6-12). Todd et al. (2011) used Nb/Yb values to map mantle heterogeneities and fertility in the south-eastern Havre Trough. Because Nb/Yb (and Nb/Y) values in most Colville Ridge lavas overlap with the range defined by the Havre Trough lavas, both regions show a similar degree of Nb/Y mantle heterogeneity, independent of subduction input.

Similarly, as Nd is rather immobile in aqueous fluids (e.g., Kessel et al., 2005), the low $^{143}Nd/^{144}Nd$ values in the Colville lavas either require input of Pacific sediment-derived melts, bulk mass transfer, or pre-existing heterogeneities in the Indo-Australian mantle flowing eastward form beneath the South Fiji Basin.

5.4 Influences from surrounding geotectonic features

We will now summarize the geochemistry of South Fiji Basin, Northland Plateau and Three Kings Ridge lavas; considering them to be parts of the regional tectonic evolution that likely affected the petrogenesis of the Colville Ridge lavas.

5.4.1 South Fiji Basin – a potential mantle contribution

Volcanic rocks recovered from the South Fiji Basin (SFB) can be grouped into three types including; a) late Oligocene back-arc basin-type lavas from the Minerva Basin (see section 2), b) Early Miocene high-K shoshonites, and c) Mid-Miocene ocean island-type lavas (e.g., Mortimer et al., 2007; Todd et al., 2011). The back-arc basin-type lavas are basalts that show some enrichments of fluid mobile elements (e.g., Rb, Ba and Pb) compared to N-MORB and subtle negative Nb and Ta anomalies. Little subduction (slab)-influence, however, is seen in the isotope data: $^{87}Sr/^{86}Sr$ <0.7028, $^{206}Pb/^{204}Pb$ = 18.4-18.75 and $^{143}Nd/^{144}Nd$ > 0.512305. The ocean island basalt (OIB)-type lavas (including the two lavas recovered from a seamount directly west of the Colville Ridge at ~33.5˚S) show typical 'concave up' trace element patterns with relatively high Nb and Ta abundances (compared to N-MORB) and negative sloping REE patterns on multi-element diagrams (Fig. 6b). The OIB-type SFB lavas have relatively low $^{87}Sr/^{86}Sr$ values of > 0.7035, extend to higher $^{206}Pb/^{204}Pb$ (up to 19.4) and lower $^{143}Nd/^{144}Nd$ values (down to 0.51287) than the back-arc basin SFB lavas, with the exception of one sample that shows signs of seafloor alteration (e.g., P_2O_5 = 6.5 wt.%). Lavas with high $^{206}Pb/^{204}Pb$ also have high Nb, Ta, LREE, Ce/Yb, Th/Zr, Nb/Y and low $^{143}Nd/^{144}Nd$ values, suggesting partial melting of a source with a trace element composition similar to that of average global OIB (Fig. 6b; Sun and McDonough et al., 1989). By contrast, the shoshonites have high LILEs (e.g.,

Ba up to 3200 ppm) and low Nb values, characteristic of a subduction-related origin. Mortimer et al. (2007) linked these lavas to an early Miocene arc rifting process, but unfortunately, no published isotope data exist from these lavas.

Lavas from the SFB therefore late-Oligocene to early-Miocene back-arc basin lavas from the Minerva plain (Fig. 1) and younger early- to mid-Miocene shoshonitic and ocean island-type volcanism in the Kupe plain (Fig. 1). The wide range in isotopic composition of these lavas is consistent with a heterogenous mantle underlying the SFB. Since the central part of the Kupe Plain is covered by sediments hindering the recovery of samples from the oceanic crust in this region, the available samples are therefore restricted to seamounts and ridges, located at the eastern and western margins of the Kupe Plain and these may not necessarily reflect the composition of the seafloor in the central Kupe plain. Nonetheless, if largely trench-perpendicular mantle (or corner) flow was operating beneath South Fiji Basin and proto-Kermadec arc, then a slightly depleted version of the SFB mantle (forming the SFB crust and seamounts) flowed eastward and represents the 'parental' mantle for the Colville/Kermadec proto-arc and possibly also for the Quaternary Havre Trough - Kermadec arc system, as proposed by Todd et al. (2010; 2011; 2012). Similar longitudinal opening rates between ~30-35˚S latitudes in the Late Oligocene - Early Miocene (e.g., Malahoff et al., 1982; Sdrolias et al., 2003; Bassett et al., 2016) support the idea of largely trench-perpendicular driven mantle flow. Therefore, it is likely that the mantle wedge beneath the Miocene proto-arc (Colville and Kermadec Ridges) contained potassic and OIB-type domains, which may still be present beneath the Havre Trough back-arc and Kermadec arc front today at similar latitudes.

5.4.2 Role of the South Fiji Basin, Northland Plateau and Three Kings Ridge mantle in the southern Kermadec and Colville proto-arc petrogenesis

Before we can reliably discuss what influence the heterogeneous mantle has on the petrogenesis of the proto-arc Kermadec and Colville lavas, we need to establish the composition of the mantle, prior to subduction input. Based on South Fiji Basin and Havre Trough back-arc lava samples least affected by slab component addition (i.e., LILEs, Th and LREEs values, similar to MORB), Todd et al. (2010; 2011) estimated the Sr-, Nd-, Pb-, and

Hf-isotopic and trace element compositions of the local least-modified mantle were similar to the enriched end member of the depleted mantle after Workman and Hart (2005). Because Sr, Nd and Pb isotopic composition of the Havre Trough and depleted South Fiji Basin back-arc lavas are similar to each other, the back-arc type mantle end-member isotopic composition is likely similar to that defined by Todd et al. (2011). Using the back-arc end-member composition similar to that defined by Todd et al. (2011), input of 1-3% of locally subducted sediment (with a similar composition to sediments being subducted today) into depleted SFB back-arc type mantle can explain the Sr- and Pb-isotopic compositions of the Colville Ridge lavas, as noted above (Fig. 11). 1-3% of sediment input via sediment melts or supercritical fluids could also account for the observed $^{143}Nd/^{144}Nd$ and Th/Zr values in some Colville and Kermadec Ridge lavas (e.g., Kessel et al., 2005).

An additional explanation of the low $^{143}Nd/^{144}Nd$ and high La/Sm, Ce/Yb and Th/Zr values of the Colville and Kermadec Ridge lavas is to include pre-existing mantle wedge heterogeneities (i.e., from back-arc basin-type to OIB-type material) as recorded by the SFB lavas. Some of these OIB-type lavas have similar Ce/Yb and Th/Zr values to the Colville Ridge lavas and span a range of $^{143}Nd/^{144}Nd$ ratios from ~0.5128-0.5131 (Fig. 9, 11-12). However, about half of the Colville (and less of the Kermadec) Ridge lavas have relatively high Ce/Yb and Th/Zr requiring additional contribution of another component with high Ce/Yb and Th/Zr, but with similar $^{143}Nd/^{144}Nd$ values. Potassic shoshonitic lavas from the South Fiji Basin and Three Kings Ridge contain high Th (and Ce in the potassic SFB lavas) contents and have significantly higher Th/Zr (and Ce/Yb in the potassic SFB lavas) values (Mortimer et al., 1998 and Mortimer et al., 2007) that can act as an additional end-member to explain the high Th/Zr values in some of the Colville and Kermadec Ridge lavas. Binary mixing between $^{143}Nd/^{144}Nd$ and Th/Zr show that ≤ 4% input of a Three Kings Ridge-type shoshonitic signature into a SFB back-arc basin-type mantle (containing subduction-derived sediment signature ± OIB-domains) can explain the observed variation in $^{143}Nd/^{144}Nd$ vs. Th/Zr values (Fig. 12) and in the $^{206}Pb/^{204}Pb$ vs. $^{87}Sr/^{86}Sr$ or $^{143}Nd/^{144}Nd$ or $^{207}Pb/^{204}Pb$ (Fig. 11a-11c). The formation of shoshonites in oceanic arc settings have previously been attributed to early oceanic arc rifting (e.g., Fiji;

Gill and Whelan, 1989). More specifically, Leslie et al. (2009) interpreted the late Miocene-Early Pliocene Fijian shoshonites as having formed via low-degrees of partial melting of metasomatised sub-arc lithosphere, prior to arc fragmentation and back-arc formation. Mortimer et al. (2007) came to a similar conclusion that the Late Eocene to Early Miocene Three Kings Ridge and Northland Plateau shoshonites are precursors of imminent arc breakup and South Fiji Basin formation. However, the occurrence of much younger (~20 Ma) shoshonites in the central-southern SFB is somewhat puzzling, although it could represent a re-melting event of metasomatised sub-arc lithosphere. The presence of a 'shoshonitic' geochemical signature in some Kermadec and Colville Ridge proto-arc lavas corroborates the Three Kings and Colville Ridges having once formed a single arc that split initiating the opening of the South Fiji Basin in the late Miocene. Although the Kermadec and Colville Ridge lavas have largely distinct isotopic compositions from the Quaternary Kermadec Arc and back arc (best seen on the $^{206}Pb/^{204}Pb$ versus $^{143}Nd/^{144}Nd$ isotope diagram), there is some overlap with the Quaternary arc samples. On each isotope diagram, the overlap could be explained by mixing or derivation from a component similar to the TKR shoshonite samples. The involvement of a TKR shoshonitic component can most clearly be seen on the $^{143}Nd/^{144}Nd$ vs Th/Zr diagram, which shows that there may be up to ~4% of such a component in the proto-arc lavas. Thus, a combination of geochemical sub arc mantle heterogeneities and element influx from the subducting sediments on the Pacific plate are required to explain the geochemical composition of the Colville and Kermadec proto-arc lavas, as compared to the Quaternary arc and back arc lavas; processes that need to be understood to understand the geochemical composition of arc lavas globally.

6. Conclusions

Fifty-three rock (lava) samples have been recovered from the southern part (south of ~33˚S) of the ~1300 km long Colville (*n* = 25) and Kermadec (*n* = 28) Ridges that bound the Kermadec arc front and Havre Trough back-arc regions. Four plagioclase separates gave ages of 6.9 ± 1.4 Ma (inverse isochron age; 7.5 ± 2.0 Ma plateau age), 3.80 ± 0.33 Ma and 2.63 ± 0.23 Ma from Colville Ridge lavas and 3.40 ± 0.24 Ma from a Kermadec Ridge lava.

An additional three groundmass $^{40}Ar/^{39}Ar$ analyses gave ages of 4.41±0.35, 4.6±1.6 and 4.8±1.2 Ma. These ages fill existing gaps between 16.7 and 2 Ma in the temporal evolution of the Colville and Kermadec Ridges. The ages furthermore demonstrate the occurrence of contemporaneous volcanism at the Colville and Kermadec Ridges between 8 and 3 Ma, and that volcanism at the Colville Ridge occurred ~2.8 Ma longer than previously known. Except for two mildly alkaline lavas from a seamount west of the Colville Ridge (TAN1512 DR11-1 and DR11-2) all lavas range in composition from low-to-medium-K picro-basalts to andesites (SiO_2 = 44.6 – 56.7 wt.%) with arc-type minor and trace element patterns (negative Nb and Ta anomalies and positive LILE contents).

Differences exist between the Kermadec and Colville Ridge lavas. The Kermadec Ridge lavas extend to higher Ba/Th and lower La/Sm, Nb/Y, Ce/Yb, Nb/Yb and Th/Yb ratios and overall have slightly less radiogenic Sr and more radiogenic Nd isotopic compositions than the Colville Ridge lavas. These geochemical differences can be explained by the transport of slab components to the Kermadec arc front mantle via hydrous fluids, whereas melts from subducted sediments were also added to the Colville rear arc mantle. The overall similarity in geochemical composition and distinct compositions from the Quaternary Kermadec arc/back arc lavas are consistent with the Kermadec and Colville Ridges having formed a single proto-Kermadec (Vitiaz) arc in the mid Miocene to Pliocene.

When compared to the Quaternary Kermadec arc front, most Kermadec and Colville Ridge lavas have similar major element compositions (except for some low-silica lavas from a seamount behind the Colville Ridge), but trend towards higher La/Sm, Nb/Y, Nb/Yb, Th/Yb and lower Ba/Th and $^{206}Pb/^{204}Pb$ (for a given Sr, Nd or $^{208}Pb/^{204}Pb$) isotope ratio. Therefore, an additional component is required in the Quaternary Kermadec arc front and back arc lavas, which could be the subducting HIMU-type Hikurangi seamounts. Therefore, there is some question as to whether the Hikurangi Plateau and seamounts also subducted beneath the Miocene-Pliocene Kermadec proto-arc, as is presently the case beneath the Kermadec Arc. Finally, high Th/Zr ratios and elevated Pb isotope ratios in some Kermadec and Colville lavas, similar to those found in Oligocene-Miocene shoshonites from Three Kings

Ridge, suggests that some enriched, shoshonitic type source mantle were also present beneath the proto-arc and the present-day Kermadec Arc. Existence of these enriched more alkaline domains profoundly affect melting behavior beneath the Kermadec arc, a process that is likely to apply to all arcs globally.

Acknowledgements

The authors would like to thank the crew and captain of R/Vs *Tangaroa* and Sonne for expert support and help during the Nirvana (TAN1213), Colville I (TAN1313), Colville II (TAN1512) and VITIAZ (SO255) expeditions. We thank Jan Sticklus, Karin Junge, Silke Hauff and Ina Simon for their assistance with the $^{40}Ar/^{39}Ar$ analyses and sample preparation at GEOMAR and Sonja Bermudez at GNS Science. Funding for the isotope measurements of the TAN1313 samples was provided by an NSERC Discovery Grant to BLC. Fruitful discussions with Rick Herzer, James Gill, Hannu Seebeck, Reinhard Werner and Erin Todd of earlier versions of this work helped to shape the ideas. KH, FH and JAW acknowledge funding from the German Federal Ministry of Education and Research (BMBF; grant #03G0255A for the SO255-Vitiaz project) and GEOMAR. CT, CdR, FCT and NM have been funded from grants made by the New Zealand Ministry of Business, Innovation and Education to GNS Science. Part of this work was funded by the European Union's Horizon 2020 research and innovation programme under the Marie Skłodowska-Curie grant agreement #79308 to CT.

Figure captions

Figure 1. Bathymetric map (Smith and Sandwell (1997) and available multi-beam data showing names of the regional geotectonic features. Symbols mark the sampling locations and with the different symbol types refer to different rock-types recovered (modified after Mortimer et al., 2007). Numbers next to the samples are published ages (in Ma) after Adams et al (1994), Mortimer et al. (1998), Ballance et al. (1999), Mortimer et al. (2007) and this study (bold letters).

Figure 2: A) Bathymetric map of the Colville Ridge south of ~32.8˚S collected during the Colville I (TAN1313) and Colville II (TAN1512) expeditions with R/V *Tangaroa* and B) of the Kermadec Ridge south of ~32.5˚S. Data used in the Kermadec Ridge map were collected during several expeditions, including SO135, SO192-1, ROVARK07, SO255 with R/V *Sonne* and TAN1104 with R/V *Tangaroa*. White circles mark sampling locations with their sampling ID number and $^{40}Ar/^{39}Ar$ age presented

here.

Figure 3: Age spectra derived from laser step-heating apparent ages and assigned errors of plagioclase separates and microcrystalline matrix. Errors are stated in 2σ. See Table 2, text and supplementary files 2 and 3 for more details.

Figure 4: Histogram showing available age data from New Zealand offshore arc lavas. Rectangles with solid lines represent $^{40}Ar/^{39}Ar$ ages and rectangles with thin dashed lines represent K-Ar age data. Data sources are: Adams et al. (1994) = Colville Ridge K-Ar age; Mortimer et al. (1998) = Three Kings Ridge, Norfolk Ridge and Basin; Ballance et al. (1999) = Kermadec Ridge and Havre Trough K-Ar ages; Mortimer et al. (2007) = South Fiji Basin; Northland Plateau and Havre Trough; Mortimer et al (2009) = Northland Plateau and Colville Ridge; Zohrab (2017) = Havre Trough and this study = Colville and Kermadec Ridge. Top panel: grey dashed lines show the duration of arc volcanism on or near the North Island of New Zealand for comparison. Data sources are: Hayward et al. (2001) = Northland arc K-Ar ages; Briggs et al. (2005) = Western Central Volcanic Zone; Skinner (1986), Adams et al. (1994), Brathwaite and Christie (1996) = Coromandel Volcanic Zone.

Figure 5: A) Plot showing a total alkali diagram (wt.% SiO_2 versus Na_2O+K_2O) after LeMaitre et al. (2002). The Colville Ridge lavas range in composition from picro-basalts to high-silica basaltic andesites. Blue diamond mark the Colville Ridge data published by Todd et al (2011) and green diamonds are Kermadec Ridge data from Wysoczanski et al (2012). Pink circles are data from South Fiji Basin lavas (Mortimer et al., 2007; Todd et al., 2011). Grey diamonds represent published whole-rock data from the following Kermadec arc front volcanoes: Clark (Gamble et al., 1997; Haase et al., 2002); Tangaroa (Todd et al., 2011); Rumble V (Todd et al., 2011); Rumble IV (Turner et al., 1997; Todd et al., 2011); Rumble III (Turner et al., 1997); Rumble II East and West (Timm et al., 2016). Brothers (Haase et al., 2002; Haase et al., 2006; Timm et al., 2012); Healy (Barker et al., 2013); Sonne (Haase et al., 2002) and northern Kermadec arc (Timm et al., 2011; and Timm et al., 2012). Small orange circles mark samples from the Havre Trough back arc (Haase et al., 2002; Todd et al., 2010; and Todd et al., 2011) B) Plot showing wt.% SiO_2 versus wt.% K_2O. Most Colville and Kermadec Ridge lavas fall in the calc-alkaline, medium-K series as defined by Gill (1981).

Figure 6: Plots showing wt.% MgO versus A) wt.% SiO_2, B) wt.% TiO_2, C) wt.% Al_2O_3, D) wt.% FeO^t, E) wt.% CaO, F) wt.% Na_2O and G) wt.% K_2O. Additional data from the South Fiji Basin (Mortimer et al., 2007; Todd et al., 2011), Northland Plateau (Mortimer et al., 2007) and Three Kings Ridge (Mortimer et al., 1998) are also shown. Other symbols and data sources are listed in the Fig. 3 caption. Grey arrows in the plots show trends consistent with crystal accumulation. BABB = Back-arc basin; SFB = South Fiji Basin.

Figure 7: Plots showing minor and trace elements distribution on multi-element diagrams normalised to a normal-mid-ocean ridge basalt (N-MORB) composition, after Sun and McDonough (1989). A) Plot showing a multi-element diagram of the Colville and Kermadec Ridge lavas. The grey field outlines the Kermadec arc front volcanoes data and the orange field marks the spectrum of trace and minor element compositions of the Havre Trough lavas (data sources are as listed in figure caption 3). B) Plot showing NMORB-normalised minor and trace element distributions of the mildly alkaline ocean island basalts (OIB)-lavas from a seamount west of the Colville Ridge. The 3 different coloured fields show the trace and minor element compositions of the different lava compositions found in the South Fiji Basin (SFB

potassic lavas = dark grey field; OIB-type lavas = medium grey field; back-arc basin (BABB)-type lavas = light grey field). Data sources are Mortimer et al. (2007) and Todd et al. (2011).

Figure 8: Plot showing $(La/Sm)_{Npm}$ ($_{Npm}$ = primitive mantle normalised after McDonough and Sun, 1995) versus Ba/Th. Data sources are as listed in Figure caption 3. The brown field shows data for sediments on the Pacific Plate (Gamble et al, 1996; Todd et al., 2010), the green field shows Hikurangi seamounts data (Smts; Mortimer and Parkinson, 1996; Hoernle et al., 2010), and the grey field are data from the Hikurangi Plateau basement (HP; Hoernle et al., 2010). The upwards pointing arrow indicates the effect of fluid-flux derived from the subducted Pacific Plate. The grey arrow pointing to the right marks the influence of mantle fertility (melting of high-Nb domains).

Figure 9: Plot of Nb/Y versus Ce/Yb. Data sources are as listed in the captions of Figures 3, 4 and 6. Upwards directed arrows point towards two potential end-member compositions: A) potassic South Fiji Basin lavas (high Ce/Yb and moderate Nb/Y values), and B) OIB-type South Fiji Basin lavas (high Nb/Y and moderate Ce/Yb values). Most Colville and Kermadec Ridge lavas fall onto an array between the South Fiji Basin back-arc basin lavas and the potassic lavas.

Figure 10: Diagram panels showing A) Nb/Yb versus Th/Yb and A) Nb/Yb versus TiO_2/Yb modified after Pearce (2008). Data sources are as listed in the captions of Figures 3, 4 and 6. B) Only lavas with < 55 wt.% SiO_2 are shown to minimise the effect of TiO_2 fractionation.

Figure 11: Plots showing $^{206}Pb/^{204}Pb$ versus A) $^{87}Sr/^{86}Sr$, B) $^{143}Nd/^{144}Nd$, C) $^{207}Pb/^{204}Pb$ and D) $^{208}Pb/^{204}Pb$. Subducting sediment data (brown field) are from Gamble et al. (1996) and Todd et al. (2010), Hikurangi Plateau data (grey field) are from Mortimer and Parkinson (1996), Hoernle et al. (2010; least altered) and Timm et al (2014; most altered) Hikurangi Seamount (HS; light yellow field) data are from Hoernle et al (2010). The shading of the Hikurangi Plateau field relates to different levels of alteration of the analysed samples with dark grey representing and pale grey indicating less alteration. Light blue circles represent near-trench samples from the Pacific Plate between 24˚ and 32˚S (Castillo et al., 2009) and the Osbourn Trough (Worthington et al., 2006). The average Pacific mid ocean ridge basalt (MORB) value is shown as a large grey star (after Meyzen et al., 2007).

Figure 12: Plot of $^{143}Nd/^{144}Nd$ versus Th/Zr. Data sources for the fields are listed in caption of Figures 3, 4 and 8. The brown finely dashed line represents mixing between a lava with a geochemical composition similar to a South Fiji Basin back-arc basin basalt and average subducting sediments on the Pacific plate ($3\%_{SSed}$). White circles and the red dashed line mark the percentage of the fertile mantle component (Three Kings Ridge (TKR) high-K domain ($3\%_{TKR}$ and $10\%_{TKR}$; Mortimer et al., 1998) added to depleted SFB back-arc basin (Todd et al., 2011). Some of the Colville and Kermadec Ridge lavas plot on the modelled trajectory between the South Fiji Basin and Three Kings Ridge shoshonites.

Table 1: Major and trace element analyses, sampling location, coordinates and water depth of the Colville and Kermadec Ridge and South Fiji Basin lavas presented in this contribution.

Table 2: Results of the $^{40}Ar/^{39}Ar$ measurements. Lab. ID # = Laboratory Identification number, MSWD = Mean Square Weighted Deviation, P = probability, SF = spreading

factor, ($^{40}Ar/^{36}Ar$)i = initial $^{40}Ar/^{36}Ar$, Wt.% = weight %, and T = temperature. Values in italics indicate statistically invalid values (i.e., SF = < 40%, or ($^{40}Ar/^{36}Ar$)i values are > or < 295.5). [a]Steps numbers associated with the degassing of fresh material are determined from the $^{36}Ar/^{37}Ar$ Alteration Index plagioclase values (Baski, 2007; Supplementary File 2). [b]Weight % K values are calculated from the combined ^{39}ArK values for each weighed sample.

Supplementary File 1: Major and trace element standard analyses as presented by Ontario Geoscience Laboratories and their deviation from GeoReM values (http://georem.mpch-mainz.gwdg.de).

Supplementary File 2: $^{40}Ar/^{39}Ar$ analytical background.

Supplementary File 3: $^{40}Ar/^{39}Ar$ run details.

Supplementary File 4: Sr, Nd and Pb isotope and trace element modelling parameters.

References

Adams, C.J., Graham, I.J., Seward, D., Skinner, D.N.B., 1994. Geochronological and geochemical evolution of late Cenozoic volcanism in the Coromandel Peninsula, New Zealand. New Zealand Journal of Geology and Geophysics 37, 359–379.

Ballance, P.F., Ablaev, A.G., Pushchin, I.K., Pletnev, S.P., Birylina, M.G., Itaya, T., Follas, H., Gibson, G.W., 1999. Morphology and history of the Kermadec trench–arc–backarc basin–remnant arc system at 30 to 32°S: geophysical profile, microfossil and K–Ar data. Marine Geology 159, 35-62.

Barker, S.J., Wilson, C.J.N., Baker, J.A., Millet-M.-A., Rotella, M.D., Wright, I.C., Wysoczanski, R.J., 2013. Geochemistry and petrogenesis of silicic magmas in the intra-oceanic Kermadec arc. Journal of Petrology 54 (2), 351-391. Doi10.1093/petrology/egs071.

Bassett, D, Sutherland, R., Henrys, S., Stern, T., Scherwarth, M., Benson, A., Toulmin, S., Henderson, M., 2010. Three-dimensional velocity structure of the northern Hikurangi margin, Raukumara, New Zealand: Implications for the growth of continental crust by subduction erosion and tectonic underplating. Geochemistry, Geophysics, Geosystems 11 (10), Q10013, doi:10.1029/2010GC003137.

Bassett, D., Kopp, H., Sutherland, R., Henrys, S., Watts, A.B, Timm, C., Scherwath, M., Grevemeyer, I., de Ronde, C.E.J. 2016. Crustal structure of the Kermadec arc from MANGO seismic refraction profiles. Journal of Geophysical Research: Solid Earth 121; 33p. doi: 10.1002/2016JB013194.

Booden, M., Smith, I.E.M., Mauk, J., Black, P.M. 2012. Geochemical and isotopic development of the Coromandel Volcanic Zone, northern New Zealand, since 18 Ma. Journal of Volcanology and Geothermal Research 219-220, 15-32.

Brathwaite, R.L. and Christie, A.B., 1996. Geology of the Waihi area, Sheet T13BD & part U13, Scale 1:50 000. Geological Map, 21. Institute of Geological and Nuclear Sciences, Ltd., Wellington, N.Z.

Brenan, J.M., Shaw, H.F., Ryerson, F.J., Phinney, D.L., 1995. Mineral-aqueous partitioning of trace elements at 900˚C and 2.0 GPa: Constraints on the trace element chemistry of mantle and deep crustal fluids. Geochimica and Cosmochimica Acta 59, 3331-3350.

Briggs, R.M., Houghton, B.F., McWilliams, M., Wilson, C.J.N. 2005. $^{40}Ar/^{39}Ar$ ages of silicic volcanic rocks in the Tauranga-Kaimai area, New Zealand: Dating the transition between volcanism in the Coromandel Arc and the Taupo Volcanic Zone. New Zealand Journal of Geology and Geophysics 48:3, 459-469.

Burnham, O.M., Schweyer, J. 2004. Inductively Coupled Plasma Mass Spectrometry at the Geoscience Laboratories: Revised capabilities due to improvements to instrumentation. Ontario Geological Survey, Open File Report 6145, p.54-1 to 54-20.

Carter, L., Shane, P., Alloway, B., Hall, I.R., Harris, S.E., Westgate, J.A., 2003. Demise of one volcanic zone and birth of another - A 12 m.y. marine record of major rhyolitic eruptions from New Zealand. Geology 31, 493-496.

Castillo, P.R., Lonsdale, P.F., Moran, C.L., Hawkins, J.W. 2009. Geochemistry of mid-Cretaceous Pacific crust being subducted along the Tonga-Kermadec Trench: Implications for the generation of arc lavas. Lithos 112, 87-102.

Cousens, B.L. (1996) Magmatic evolution of Quaternary mafic magmas at Long Valley Caldera and the Devils Postpile, California: Effects of crustal contamination on lithospheric mantle-derived magmas. Journal of Geophysical Research 101, 27673-27689.

DeMets, C., Gordon, R.G., Argus, D.F., Stein, S., 1994. Effect of recent revisions to the geomagnetic reversal time scale and estimates of current plate motions. Geophysical Research Letters 21, 2191-2194.

de Ronde, C.E.J., Baker, E.T., Massoth, G.J., Lupton, J.E., Wright, I.C., Feely, R.A., Green, R.R., 2001. Intra-oceanic subduction-related hydrothermal venting, Kermadec volcanic arc, New Zealand. Earth and Planetary Science Letters 193, 359-369.

de Ronde, C.E.J., Baker, E.T., Massoth, G.J., Lupton, J.E., Wright, I.C., Sparks, R.J., Bannister, S.C., Reyners, M.E., Walker, S.L., Greene, R.R., Ishibashi, J., Faure, K., Resing, J.A., Lebon, G.T., 2007. Submarine hydrothermal activity along the mid-Kermadec Arc, New Zealand: Large-scale effects on venting, Geochemistry Geophysics Geosystems 8 (7) Q07007, doi:10.1029/2006GC001495.

de Ronde, C.E.J., Walker, S.L., Ditchburn, R.G., Caratori-Tontini, F., Hannington, M.D, Merle, S.G., Timm, C., Handler, MR., Wysoczanski, R.J., Dekov, V.M., Kamenov, G.D., Baker, E.T., Embley, R.W., Lupton, J.E., Stoffers, P., 2014. The anatomy of a buried submarine hydrothermal system, Clark Volcano, Kermadec Arc, New Zealand. Economic Geology 109, 2261-2292.

Duncan, R.A., Vallier, T.L., Falvey, D.A. 1985. Volcanic episodes at Eua, Tonga Islands. In: Scholl, D. W. and Vallier, T. L., compilers and editors 1985, Geology and offshore resources of Pacific island arcs—Tonga region, Circum-Pacific Council for Energy and Mineral Resources Earth Science Series, v. 2: Houston, Texas, Circum-Pacific Council for Energy and Mineral Resources, ?-?.

Falloon, T., Meffre, S., Crawford, A.J., Hoernle, K., Hauff, F., Bloomer, S.H., Wright, D.J. 2014. Cretaceous fore-arc basalts from the Tonga arc: Geochemistry and implications for the tectonic history of the SW Pacific. Tectoniphysics 630, 21-32.

Fisher, A.T., Davis, E.E., Hutnak, M., Spiess, V., Zuehlsdorff, L., Cherkaoui, A., Christiansen, L., Edwards, K., Macdonald, R., Villinger, H., Mottl, M.J., Wheat, C.G., Becker, K. 2003. Hydrothermal recharge and discharge across 50 km guided by seamounts on a young ridge flank. Nature 421, 618-621.

Gamble, J.A., Wright, I.C., Woodhead, J.D., McCulloch, M.T. 1995. Arc and back-arc geochemistry in the southern Kermadec arc-Ngatoro Basin offshore Taupo Volcanic Zone, SW Pacific. From Smellie, J.L. (ed.), 1995, Volcanism Associated with Extension at Consuming Plate Margins, Geological Society Special Publication No. 81,193-212.

Gamble, J., Woodhead, J., Wright, I., Smith, I., 1996. Basalt and sediment geochemistry and magma petrogenesis in a transect from oceanic island arc to rifted continental margin arc: The Kermadec-Hikurangi Margin, SW Pacific. Journal of Petrology 37, 1523-1546.

Gamble, J.A., Christie, R.H.K., Wright. I.C., Wysoczanski, R.J., 1997. Primitive K-rich magmas from Clark volcano, southern Kermadec arc: a paradox in the K-depth relationship. Canadian Mineralogist 35, 275-290.

Garbe-Schönberg, C.-D., 1993. Simultaneous determination of thirty-seven trace elements in twenty-eight international rock standards by ICP-MS. Geostandards Newsletter 17, 81–97.

Gill, J.B., 1976. Composition and age of Lau Basin and Ridge volcanic rocks: Implications for evolution of an interarc basin and remnant arc. Geological Society of America Bulletin 87, 1384-1395.

Gill, J.B., Stork, A.L., Whelan, P.M., 1984. Volcanism accompanying back-arc basin development in the southwest Pacific. Tectonophysics 102, 207-224.

Gill, J.B., 1987. Early Geochemical Evolution of an Oceanic Island Arc and Back-arc: Fiji and the South Fiji Basin. Journal of Geology 95, 589-615.

Gill, J.B., Whelan, P., 1989. Early Rifting of an Oceanic Island Arc (Fiji) Produced Shoshonitic to Tholeiitic Basalts. Journal of Geophysical Research 94, 4561-4578.

Haase, K.M., Worthington, T.J., Stoffers, P., Garbe-Schoenberg, D., Wright, I., 2002. Mantle dynamics, element recycling, and magma genesis beneath the Kermadec Arc-Havre Trough. Geochemistry Geophysics Geosystems 3 (11) 1071, doi:10.1029/2002GC000335.

Haase, K.A., Stroncik, N., Garbe-Schoenberg, D., Stoffers, P., 2006. Formation of island arc dacite magmas by extreme crystal fractionation: An example from Brothers Seamount, Kermadec island arc (SW Pacific). Journal of Volcanology and Geothermal Research 152, 316-330.

Hastie, A.R., Kerr, A.C., Pearce, J.A., Mitchell, S.F., 2007. Classification of altered volcanic island arc rocks using immobile trace elements: development of the Th-Co discrimination diagram. Jouranl of Petrology 48 (12), 2341-2357.

Hergt, J., Woodhead, J. 2007. A critical evaluation of recent models for Lau-Tonga arc-backarc basin magmatic evolution. Chemical Geology 245, 9-44.

Herzer, R.H., Barker, D.H.N., Roest, W.R., Mortimer, N. 2011. Oligocene-Miocene spreading history of the northern South Fiji Basin and implications for the evolution of the New Zealand plate boundary. Geochemistry, Geophysics Geosystems 12 (2), Q02004, doi:10.1029/2010GC003291.

Hoernle, K., Hauff, F., Bogaard, Pvd., Werner, R., Mortimer, N., Geldmacher, J., Garbe-Schoenberg, D., Davy, B., 2010. Age and geochemistry of volcanic rocks from the Hikurangi and Manihiki oceanic plateaus. Geochimica et Cosmochimica Acta 74, 7196–7219, doi:10.1016/j.gca.2010.09.030.

Kessel, R., Schmidt, M.W., Ulmer, P., Pettke T. (2005), Trace element signature of subduction-zone fluids, melts and supercritical liquids at 120-180 km depth, Nature 437, 724-727.

Larter, R.D., Leat, P.T., 2003. Intra Oceanic Subduction Systems: Tectonic and Magmatic Processes. Geological Society, London, Special Publications, 219, 1-17.

Le Maitre, R. W. (editor), Streckeisen, A., Zanettin, B., Le Bas, M.J., Bonin, B., Bateman, P., Bellieni, G., Dudek, A., Efremova, S., Keller, J., Lamere, J., Sabine, P.A., Schmid, R., Sörensen, H., Woolley, A.R., 2002. Igneous Rocks: A Classification and Glossary of Terms, Recommendations of the International Union of Geological Sciences, Subcommission of the Systematics of Igneous Rocks. Cambridge University Press.

Leslie, R.A.J., Danyushevsky, Crawford, A.J., Verbeeten, A.C., 2009. Primitive shoshonites from Fiji: Geochemistry and source components. Geochemistry Geophysics Geosystems 10 (7), Q07001, doi:10.1029/2008GC002326.

Malahoff, A., Feden, R.H., Fleming, H.S., 1982. Magnetic anomalies and tectonic fabric of marginal basins north of New Zealand. Journal of Geophysical Research 87, 4109–4125.

McCulloch, M.T., Gamble, J.A., 1991. Geochemical and geodynamical constraints on subduction zone magmatism. Earth and Planetary Science Letters 102, 358-374.

McDonough, W.F., Sun, S.-s., 1995. The composition of the Earth. Chemical Geology 120, 223-253.

Meffre, S., Fallon, T.J., Crawford, A.J., Hoernle, K., Hauff, F., Duncan, R.A., Bloomer, S.H., Wright, D.J. 2012. Basalts erupted along the Tongan fore arc during subduction initiation: Evidence from geochronology of dredged rocks from the Tonga fore arc and trench. Geochemistry Geophysics Geosystems, v. 13, p. Q12003, doi: 10.1029/2012GC004335.

Meyzen, C.M., Blichert-Toft, J., Ludden, J.N., Humler, E., Mével, C., Abarede, F., 2007. Isotopic portrayal of the Earth's upper mantle flow field. Nature 444, doi:10.1038/nature05920.

Mortimer, N., Parkinson, D., 1996. Hikurangi Plateau: A large igneous province in the southwest Pacific Ocean. Journal of Geophysical Research 101 (B1), 687-696.

Mortimer, Herzer, R.H., Gans, P.B., Parkinson, D.L., Seward, D., 1998. Basement geology from the Three Kings Ridge to West Norfolk Ridge, southwest Pacific Ocean: evidence from petrology, geochemistry and isotopic dating of dredge samples. Marine Geology 148, 135-162.

Mortimer, N., Herzer, R.H., Gans, P.B., Laporte-Magoni, C., Calvert, A.T., Bosch, D., 2007. Oligocene–Miocene tectonic evolution of the South Fiji Basin and Northland Plateau, SW Pacific Ocean: Evidence from petrology and dating of dredged rocks. Marine Geology 237, 1-24.

Mortimer, N., Gans, P.B., Palin, J.M.,Meffre, S., Herzer, R.H., Skinner, D.N.B., 2010. Location and migration of Miocene-Quaternary volcanic arcs in the SW Pacific region. Journal of Volcanology and Geothermal Research 190, 1-10.

Parson, L.M., Hawkins, J.W. 1994. Two-stage ridge propagation and geological history of the Lau backarc basin. In: Hawkins, J., Parson, U Allan, J., et al., 1994 Proceedings of the Ocean Drilling Program, Scientific Results, Vol. 135, pp. 819-828.

Pearce, J.A., 2008. Geochemical fingerprinting of oceanic basalts with applications to ophiolite classification and the search of Archean oceanic crust. Lithos 100, 14-48.

Rowan, C.R., Roberts, A.P., 2008. Widespread remagnetizations and a new view of Neogene tectonic rotations within the Australia-Pacific plate boundary zone, New Zealand. Journal of Geophysical Research 113, B03103, doi:10.1029/2006JB004594.

Schellart, W.P., Spakman, W., 2012. Mantle constraints on the plate tectonic evolution of the Tonga-Kermadec-Hikurangi subduction zone and the South Fiji Basin region. Australian Journal of Earth Sciences 59:6, 933-952, doi:10.1080/8120099.2012.679692.

Scherwarth, M., Kopp, H., Flueh, E.R., Henrys, S.A., Sutherland, R., Stagpoole, V.M., Barker, D.H.N., Reyners, M.E., Basset, D.G., Planert, L., Dannowski, A., 2010. Fore-arc deformation at the northern Hikurangi margin, New Zealand. Journal of Geophysical Research 115, B06408, 10.1029/2009JB006645.

Sdrolias, M., Mueller, D., Gaina, C. 2003. Tectonic evolution of the southwest Pacific using constraints from back-arc basins. Geological Society of America Special Paper 372, 343–359.

Seebeck, H., Nicol, A., Giba, M., Pettingam J., Walsh, J., 2014. Geometry of the subducting Pacific plate since 20?Ma, Hikurangi margin, New Zealand. Journal of the Geological Society 171, 131-143.

Skinner, D.N.B., 1986. Neogene volcanism of the Hauraki Volcanic Region. Bulletin of the Royal Society of New Zealand 23, 21–47.

Smith, W.H.F., Sandwell, D.T., 1997. Global Sea Floor Topography from Satellite Altimetry and Ship Depth Soundings. Science 277, 1956-1962.

Sun, S.-s., McDonough, W.F., 1989. Chemical and isotopic systematics of oceanic basalts: implications for mantle composition and processes, In: Saunders, A. D. & Norry, M. J. (eds) Magmatism in the Ocean Basins, Geological Society of London Special Publications 42, 313–345.

Taylor, B., Zellmer, K., Martinez, F., Goodliffe, A. 1996. Seafloor spreading in the Lau back-arc basin. Earth and Planetary Science Letters 144, 35-40.

Timm, C., Graham, I.J., de Ronde, C.E.J., Leybourne, M.I., Woodhead, J., 2011. Geochemical evolution of Monowai volcanic center: New insights into the northern Kermadec arc subduction system, SW Pacific. Geochemistry, Geophysics, Geosystems 12 (8), Q0AF01, doi:10.1029/2011GC003654.

Timm, C., de Ronde, C.E.J., Leybourne, M.I., Layton-Matthews, D., Graham, I.J., 2012. Sources of chalcophile and siderophile elements in Kermadec arc lavas. Economic Geology 107, 1527-1538.

Timm, C., Bassett, D., Graham, I.J., Leybourne, M.I., de Ronde, C.E.J., Woodhead, J., Layton-Matthews, D., Watts, A.B., 2013. Louisville seamount subduction and its implication on mantle flow beneath the central Tonga-Kermadec arc. Nature Communications, 4, doi:10.1038/ncomms1720.

Timm, C., Davy, B., Haase, K., Hoernle, K.A., Graham, I.J., de Ronde, C.E.J., Woodhead, J., Bassett, D., Hauff, F., Mortimer, N., Seebeck, H.C., Wysoczanski, R.J., Caratori-Tontini, F., Gamble, J., 2014. Large Igneous Province subduction: Impact of the Hikurangi Plateau on the Kermadec arc. Nature Communications 5:4923, doi:10.1038/ncomms5923.

Timm, C., Leybourne, M., Hoernle, K., Wysoczanski, R., Hauff, F., Handler, M., Caratori-Tontini, F., de Ronde, C.E.J. 2016. Trench perpendicular geochemical variation between the two adjacent Kermadec arc volcanoes Rumble II East and West: role of the subducted Hikurangi Plateau on element recycling and metal transport in arc magmas. Journal of Petrology 57 (7), 1335-1360 doi:1093petrology/egw042.

Todd, E., Gill, J.B., Wysoczanski, R.J., Handler, M.R., Wright, I.C., Gamble, J.A., 2010. Sources of constructional cross-chain volcaniosm in the southern Havre Trough: New insights from the HFSE and REE concentration and isotope systematics, Geochemistry, Geophysics, Geosystems 11 (4), Q04009, doi:10.1029/2009GC002888.

Todd, E., Gill, J.B., Wysoczanski, R.J., Hergt, J., Wright, I.C., Leybourne, M.I., Mortimer, N., 2011. Hf isotopic evidence for small-scale heterogeneity in the mode of mantle wedge enrichment: Southern Havre Trough and South Fiji Basin back arcs. Geochemistry Geophysics Geosystems 12 (9), Q09011, doi:10.1029/2011GC003683.

Todd, E., Gill, J.B., Pearce, J.A. 2012. A variably enriched mantle wedge abd contrasting melt types during arc stages following subduction initialtion in Fiji and Tonga, southwest Pacific. Earth and Planetary Science Letters 335-336, 180-194.

Todt, W., R. A. Cliff, A. Hanser, Hofmann, A. W., 1984. $^{202}Pb/^{205}Pb$ spike for Pb isotopic analysis, Terra Cognita 4, 209.

Turner, S.P., Hawkesworth, C.J., Rogers, N.W., Bartlett, J., Smith, I., Worthington, T., 1997. Uranium-238/ thorium-230 disequilibria, magma petrogenesis, and flux rates beneath the depleted Tonga-Kermadec island arc, Geochimica et Cosmochimica Acta 61, 4855-4884.

van der Hilst, R., 1995. Complex morphology of subducted lithosphere in the mantle beneath the Tonga trench. Nature 374, 154-157.

Whelan, P.M., J. B. Gill, E. Kollman, R. A. Duncan, and R. E. Drake, 1985. Radiometric dating of magmatic stages in Fiji, in Geology and Offshore Resources of the Pacific Island Arcs--Tonga Region, Earth Sci. Series, edited by D. W. Scholl and T. L. Vallier, vol., 2, p. 415-440, Circum-Pacific Council for Energy and Mineral Resources, Houston, Texas

Wilson, C.J.N., Houghton, B.F., McWilliams, M.O., Lanphere, M.A., Weaver, S.D., Briggs, R.M., 1995. Volcanic and structural evolution of the Taupo Volcanic Zone, New Zealand: a review. Journal of Volcanology and Geothermal Research 68, 1-28.

Workman, R., Hart, S.R., 2005. Major and trace element composition of the depleted MORB mantle (DMM). Earth and Planetary Science Letters 231, 53-71.

Worthington, T.J., Hekinian, R., Stoffers, P., Kuhn, T., Hauff, F. 2006. Osbourn Trough: Structure, geochemistry and implications of a mid-Cretaceous paleospreading ridge in the South Pacific. Earth and Planetary Science Letters 245, 685-701.

Wright, I.C. 1997. Morphology and Evolution of the remnant Colville and active Kermadec arc ridges south of 33˚30' S. Marine Geophysical Researches 19, 177-193.

Wright, I.C., Worthington, T.J., Gamble, J.A., 2006. New multibeam mapping and geochemistry of the 30˚-35˚ S sector, and overview, of southern Kermadec arc volcanism. Journal of Volcanology and Geothermal Research 149, 263-296.

Wysoczanski, R.J., Todd, E., Wright, I.C., Leybourne, M.I., Hergt, J.M., Adam, C., Mackay, K. 2010. Backarc rifting, constructional volcanism and nascent disorganized spreading in the outhern Havre Trough backarc rifts (SW Pacific), Journal of Volcanology and Geothermal Research 190, 39-57.

Wysoczanski, R.J., Handler, M., Schipper, C.I., Leybourne, M.I., Creech, J., Rotella, M.D., Nichols, A.R.L., Wilson, C.J.N. & Stewart, R.B., 2012. The tectonomagmatic source of ore metals and volatile elements in the southern Kermadec arc. Economic Geology 107, 1539-1556.

Zellmer, K., Taylor, B., 2001. A three-plate kinematic model for Lau Basin opening. Geochemistry Geophysics Geosystems 2, 2000GC000106.

Zohrab, A.D.C., 2017. The Petrology, geochemistry and geochronology of back-arc stratovolcanoes in the southern Kermadec arc-Havre Trough, SW Pacific. Masters thesis, Victoria University of Wellington, pp. 166.

Figure 1

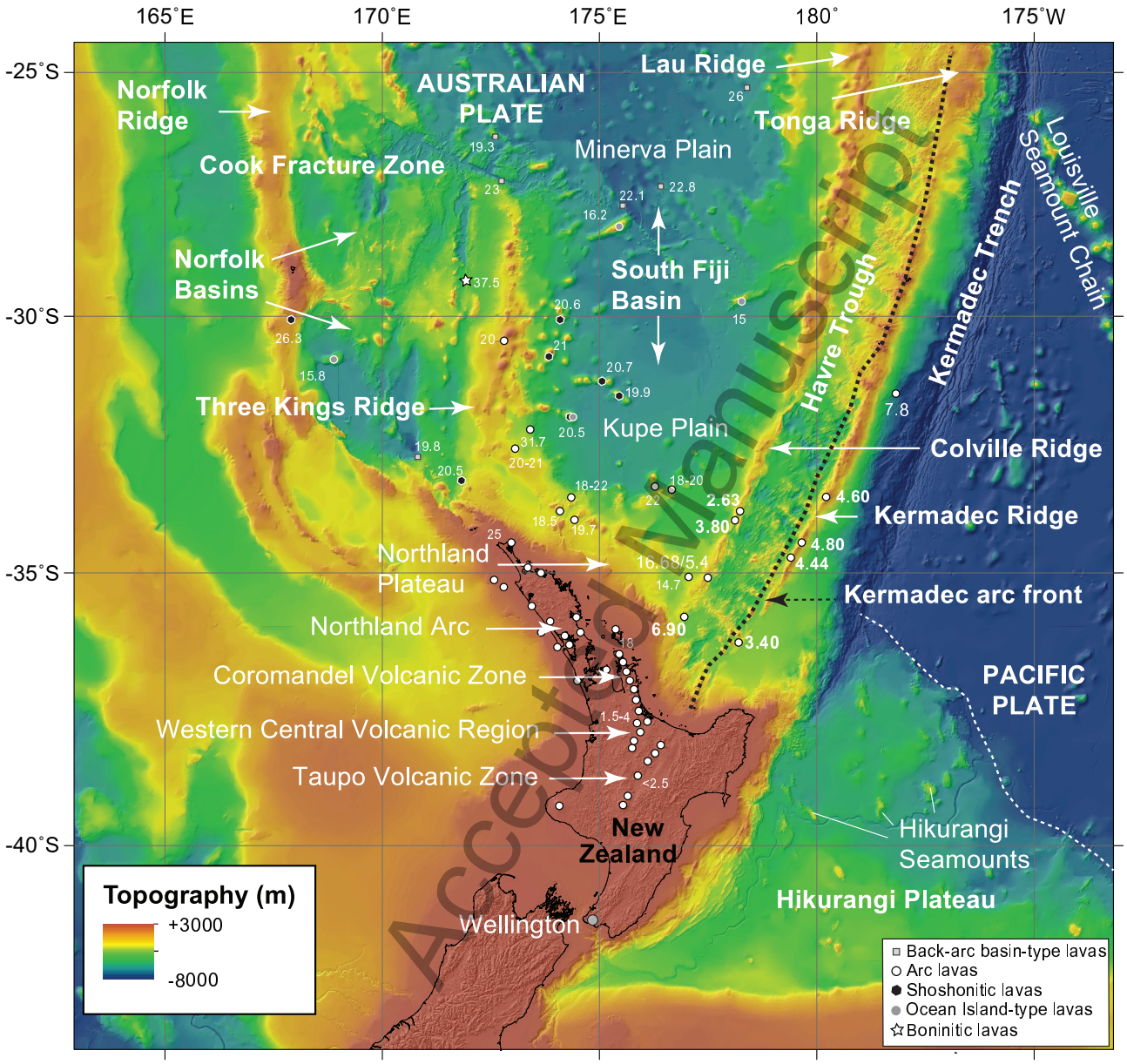
165˚E
170˚E
175˚E
180˚
175˚W
-25˚S
-30˚S
-35˚S
-40˚S
Norfolk Ridge
AUSTRALIAN PLATE
Lau Ridge
Tonga Ridge
Cook Fracture Zone
Minerva Plain
Louisville Seamount Chain
Kermadec Trench
Norfolk Basins
South Fiji Basin
Havre Trough
Three Kings Ridge
Kupe Plain
Colville Ridge
Kermadec Ridge
Northland Plateau
Kermadec arc front
Northland Arc
Coromandel Volcanic Zone
PACIFIC PLATE
Western Central Volcanic Region
Taupo Volcanic Zone
New Zealand
Hikurangi Seamounts
Hikurangi Plateau
Wellington
Topography (m)
+3000
-8000
Back-arc basin-type lavas
Arc lavas
Shoshonitic lavas
Ocean Island-type lavas
Boninitic lavas
Accepted Manuscript

Figure 2

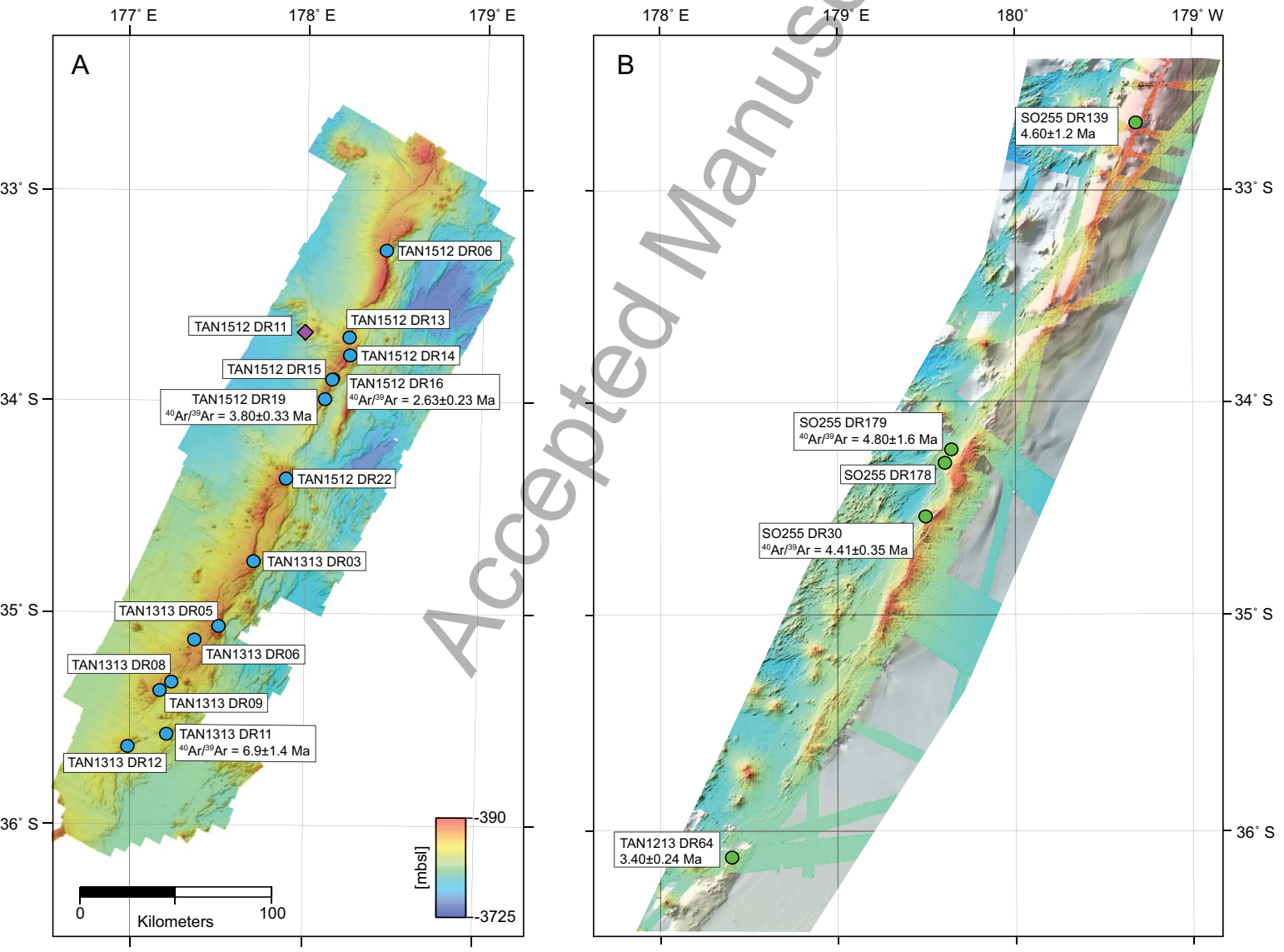

Figure 3

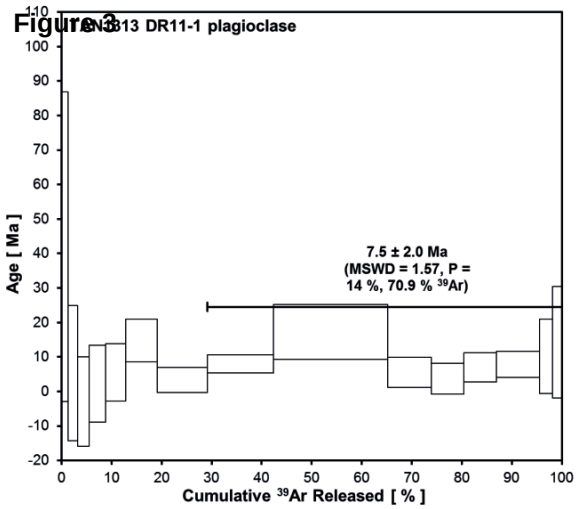

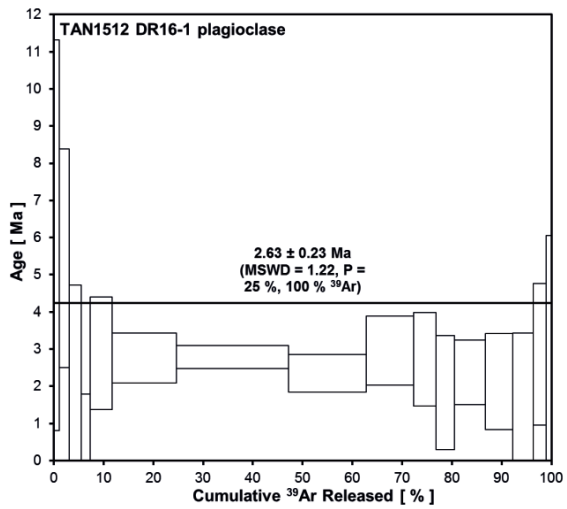

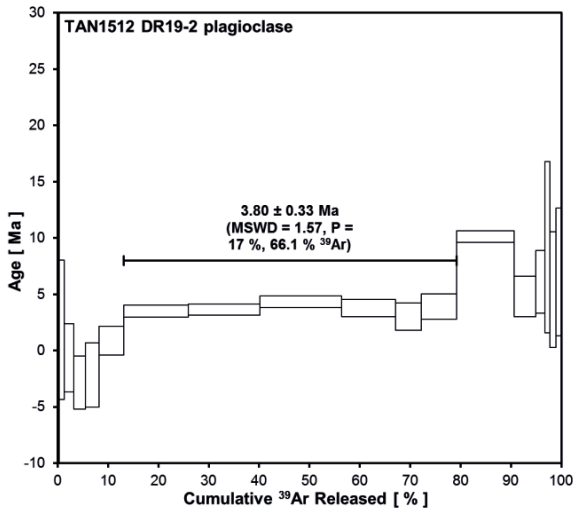

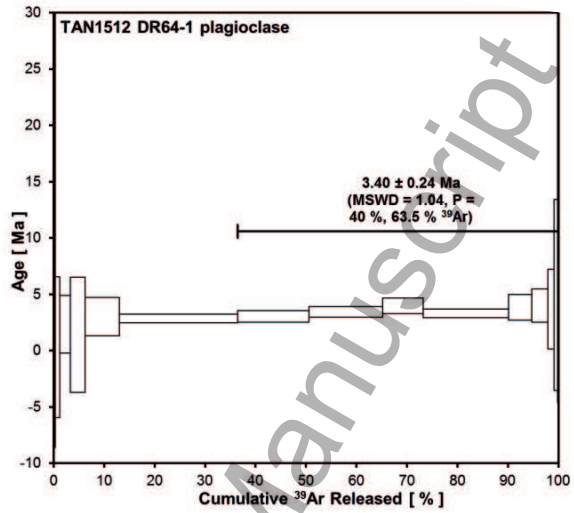

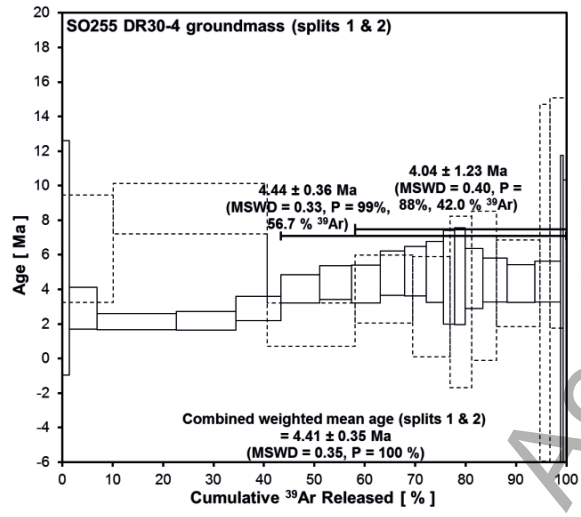

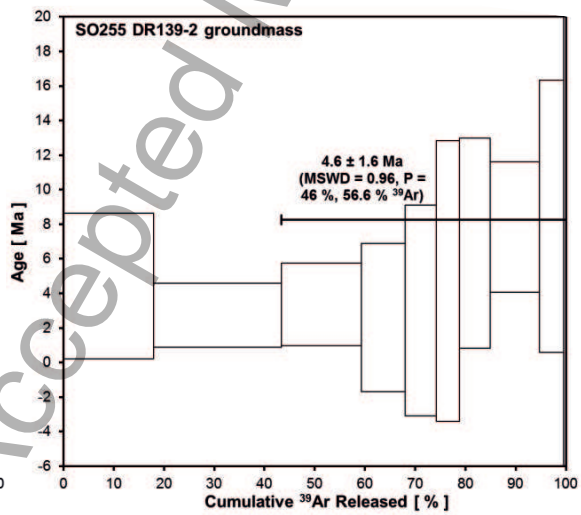

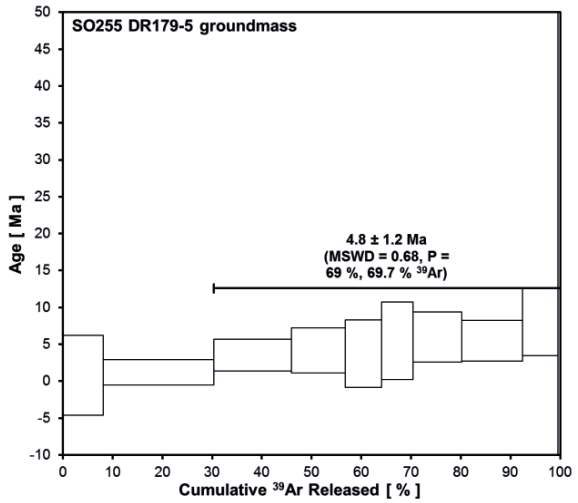

Figure 4

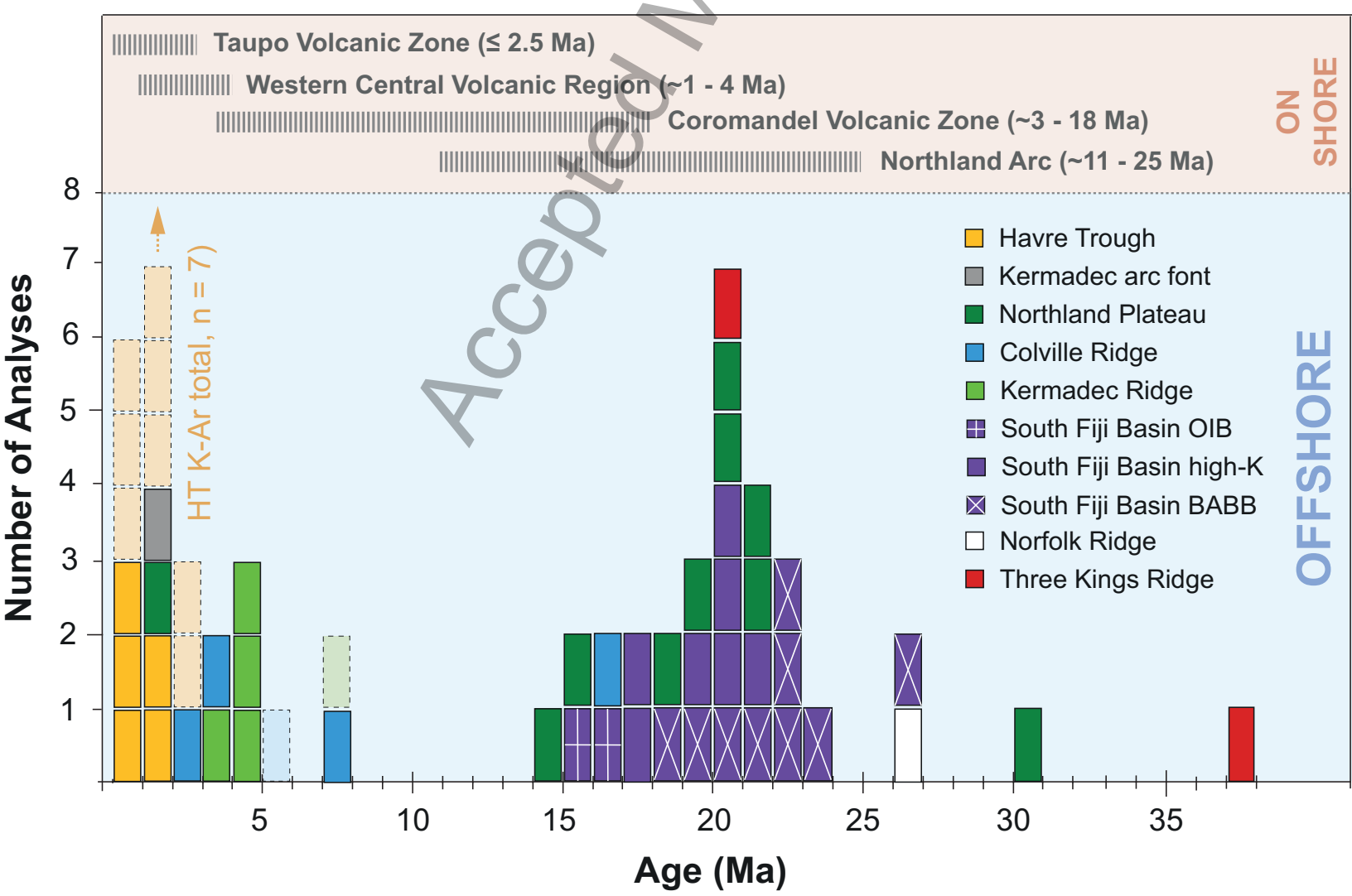

Figure 5

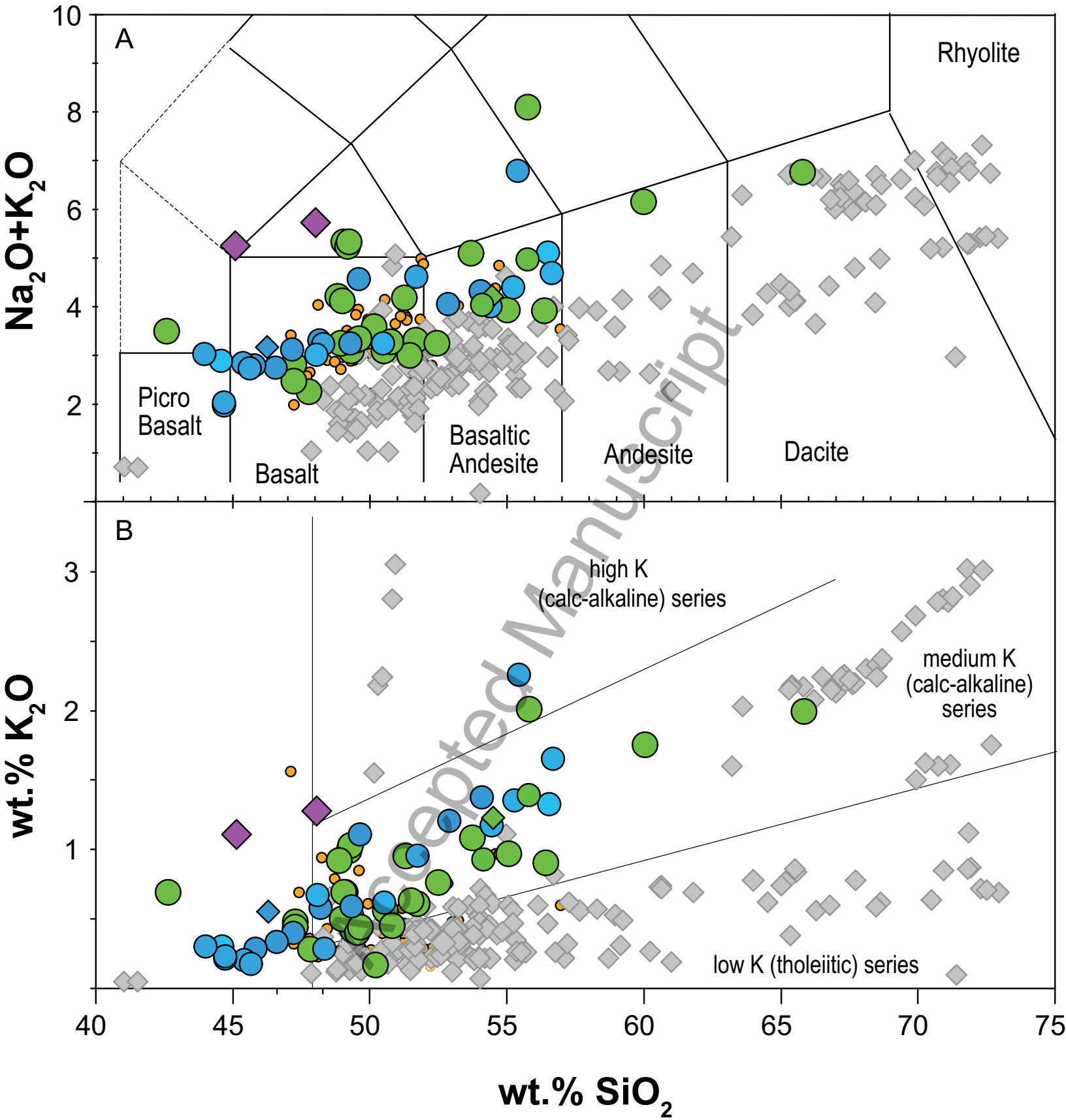

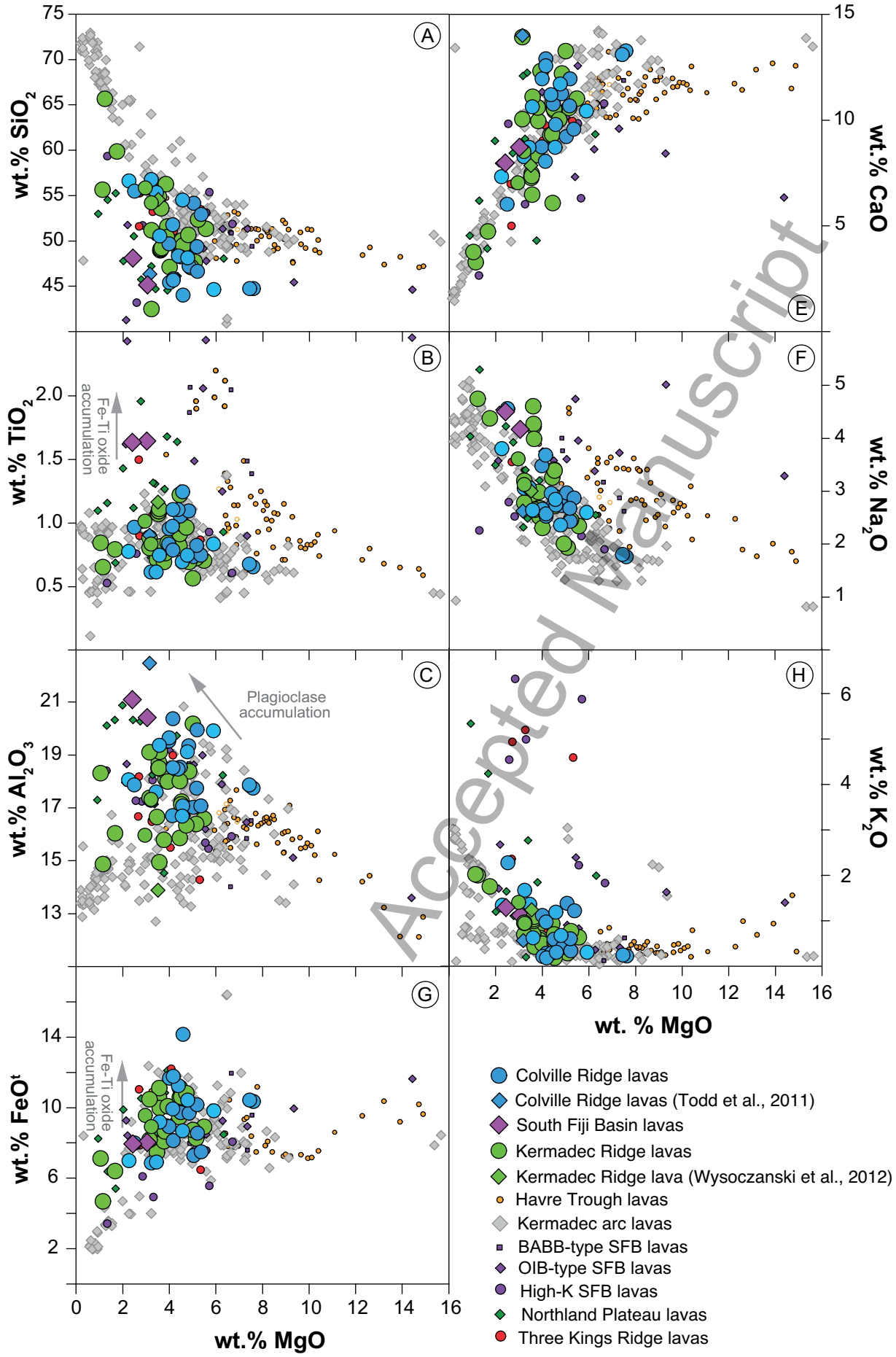

Figure 7

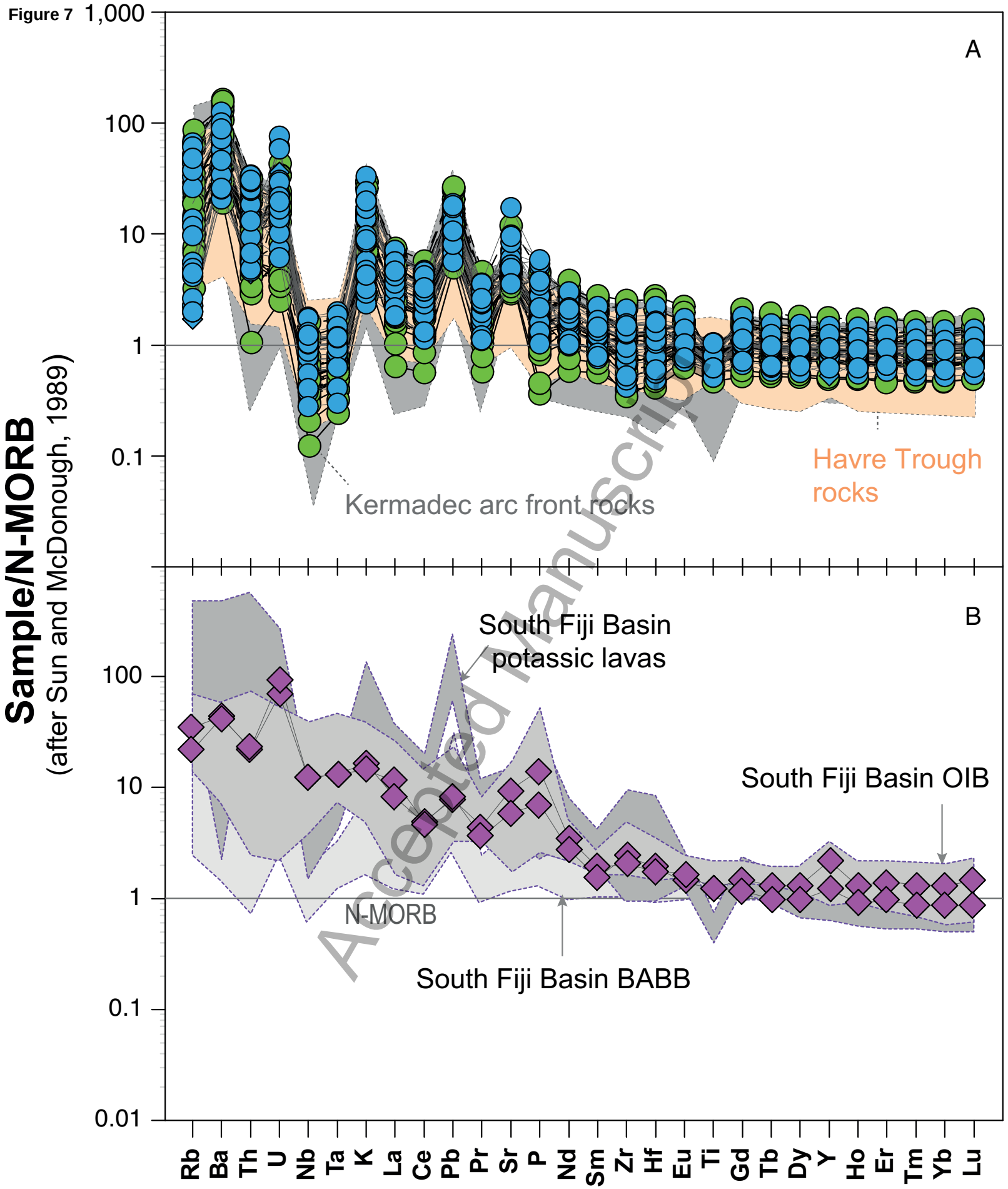

Figure 8

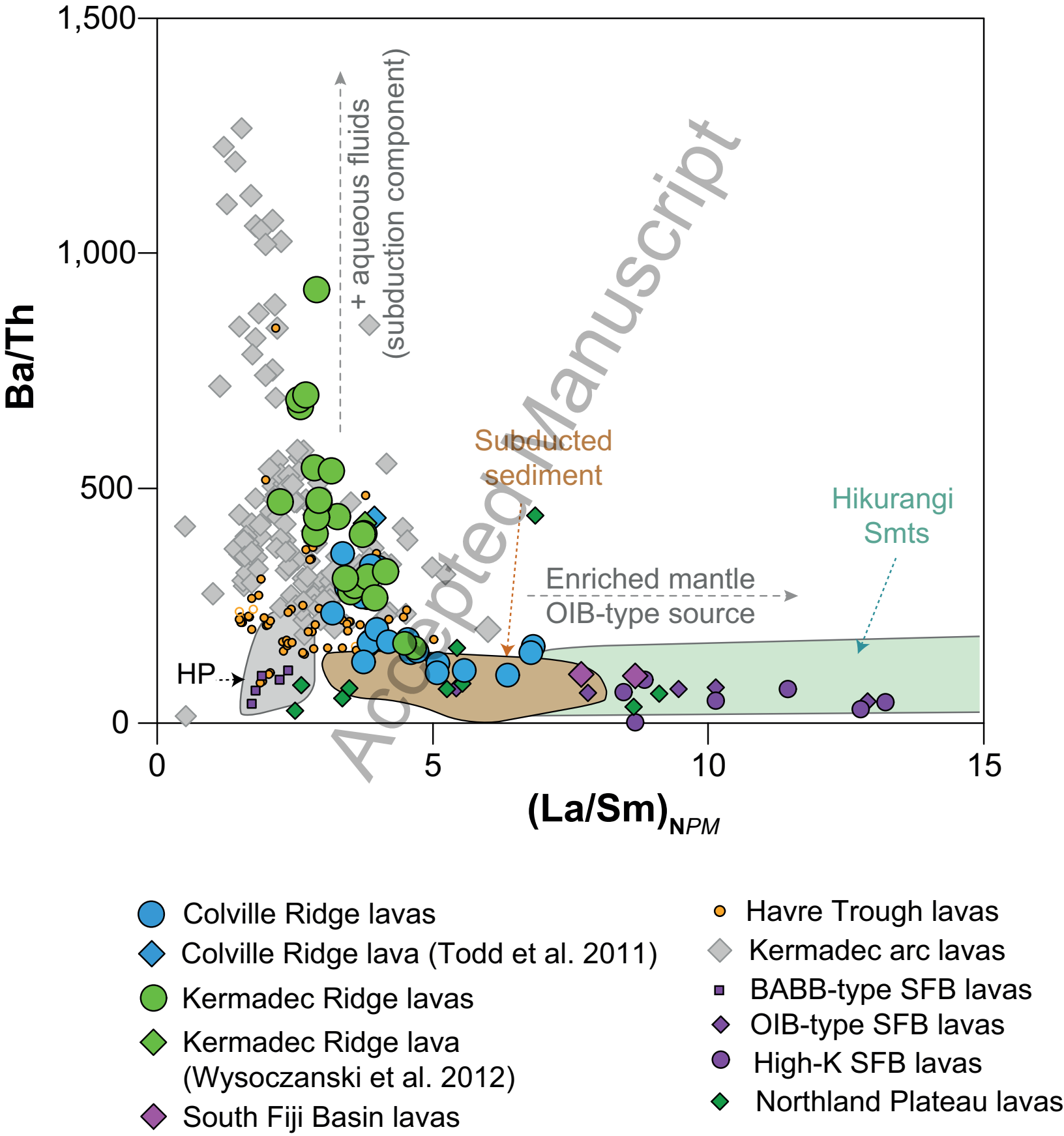
1,500
1,000
500
0
Ba/Th
0
5
10
15
(La/Sm)NPM
+ aqueous fluids
(subduction component)
Subducted
sediment
Hikurangi
Smts
Enriched mantle
OIB-type source
HP
Accepted Manuscript
Colville Ridge lavas
Colville Ridge lava (Todd et al. 2011)
Kermadec Ridge lavas
Kermadec Ridge lava
(Wysoczanski et al. 2012)
South Fiji Basin lavas
Havre Trough lavas
Kermadec arc lavas
BABB-type SFB lavas
OIB-type SFB lavas
High-K SFB lavas
Northland Plateau lavas

Figure 9

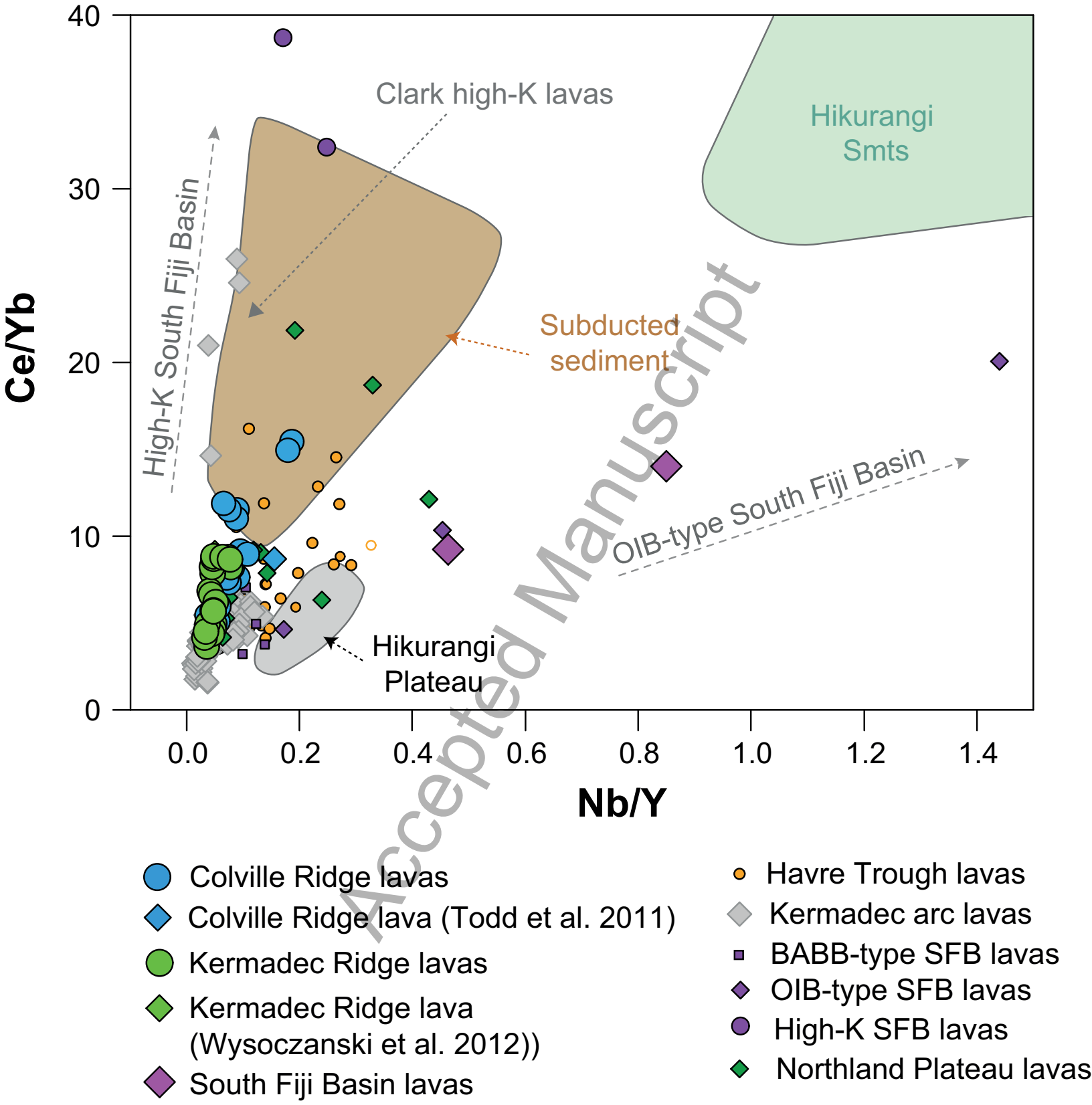

Figure 10

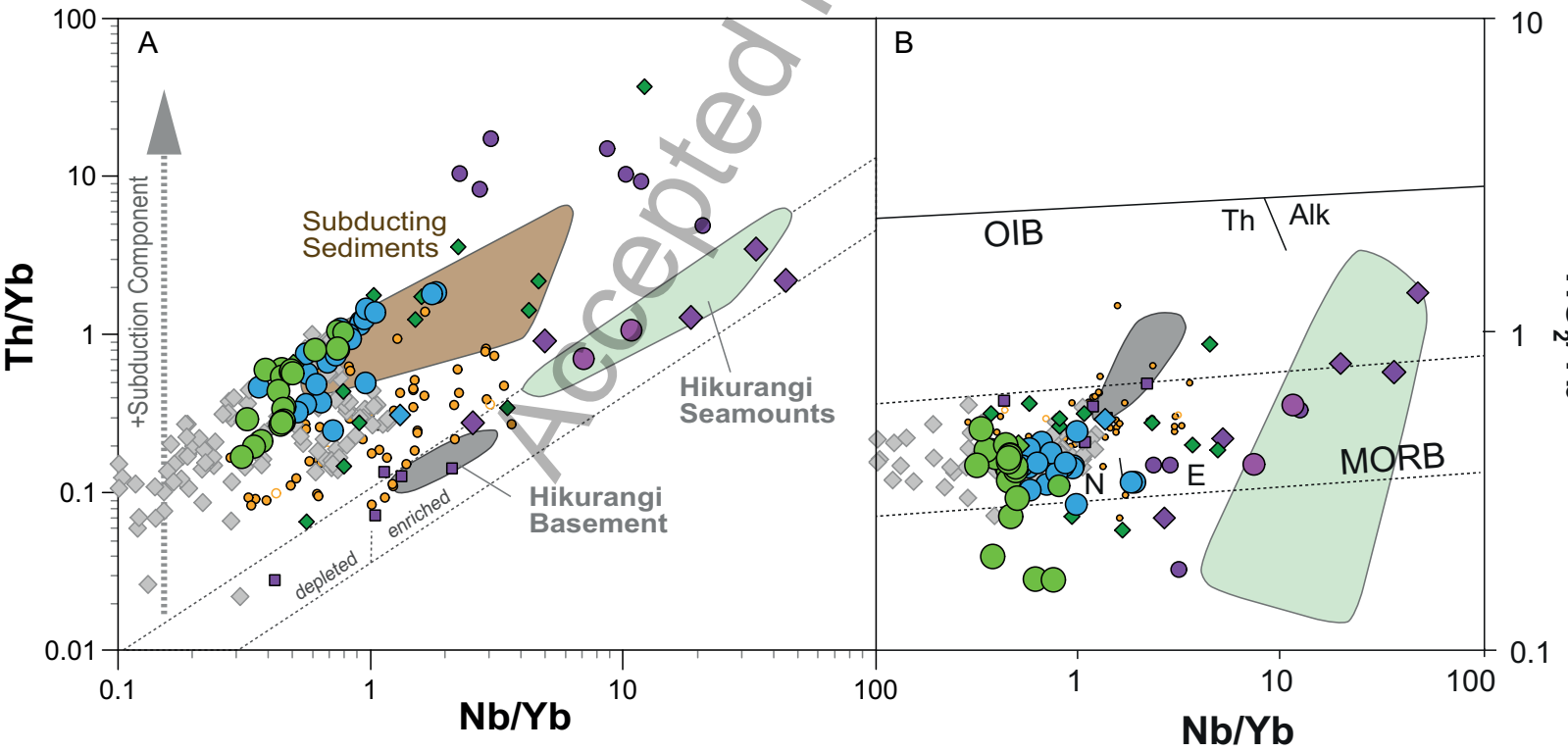

- Colville Ridge lavas
- Colville Ridge lava (Todd et al., 2011)
- South Fiji Basin lavas (this study)
- Kermadec Ridge lavas
- Kermadec Ridge lava (Wysoczanski et al., 2012)
- Havre Trough lavas
- Kermadec arc lavas
- BABB-type SFB lavas
- OIB-type SFB lavas
- High-K SFB lavas
- Northland Plateau lavas

Figure 11

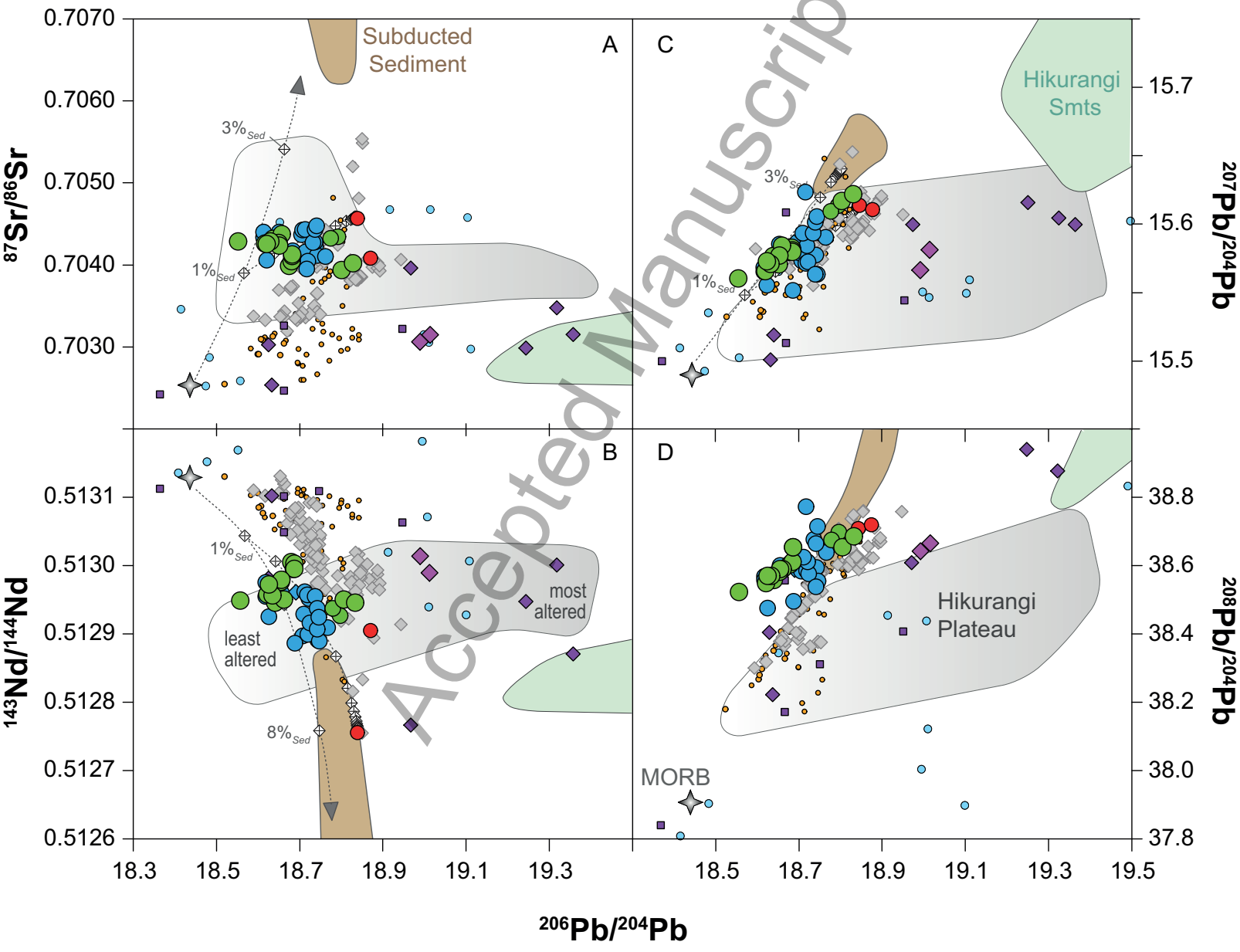

- Colville Ridge lavas
- Colville Ridge lava (Todd et al. 2011)
- Kermadec Ridge lavas
- South Fiji Basin lavas
- Havre Trough lavas
- Kermadec arc lavas
- BABB-type SFB lavas
- OIB-type SFB lavas
- Three Kings Ridge lavas
- Near-trench Pacific oceanic crust

Figure 12

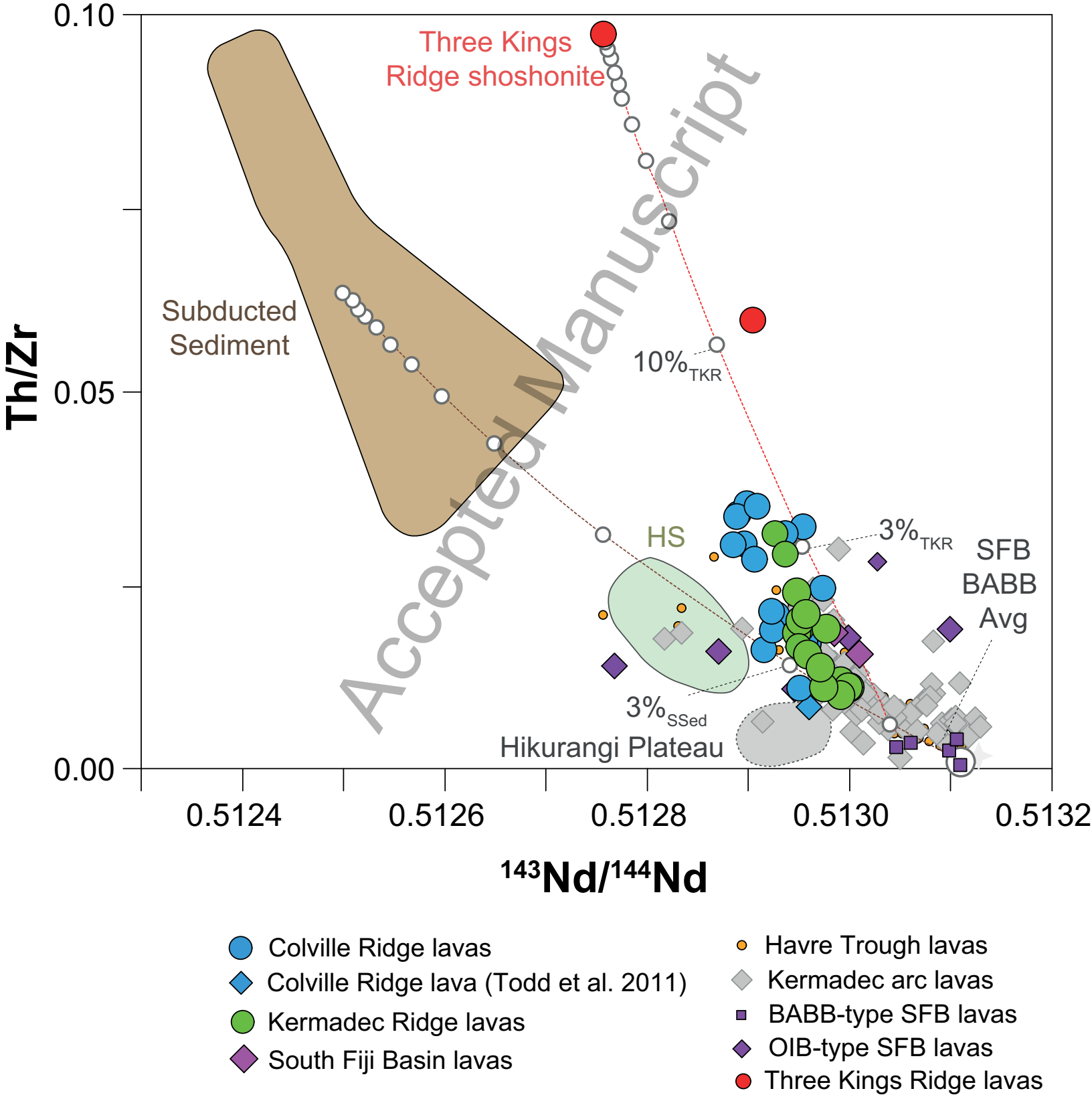
0.10
0.05
0.00
Th/Zr
0.5124
0.5126
0.5128
0.5130
0.5132
143Nd/144Nd
Three Kings
Ridge shoshonite
Subducted
Sediment
10%TKR
3%TKR
HS
SFB
BABB
Avg
3%SSed
Hikurangi Plateau
Accepted Manuscript
Colville Ridge lavas
Colville Ridge lava (Todd et al. 2011)
Kermadec Ridge lavas
South Fiji Basin lavas
Havre Trough lavas
Kermadec arc lavas
BABB-type SFB lavas
OIB-type SFB lavas
Three Kings Ridge lavas

Table 1

Table 1: Major and trace element composition of Colville Ridge lavas

Sample No.	TAN1313 DR03-1	TAN1313 DR05-1A	TAN1313 DR05-1C	TAN1313 DR06-1	TAN1313 DR06-3	TAN1313 DR08-1	TAN1313 DR08-3	TAN1313 DR09-1
Volcano	Colville Ridge	Colville Ridge	Colville Ridge	Colville Ridge	Colville Ridge	Colville Ridge	Colville Ridge	Colville Ridge
Location	Upper ridge flank	Upper ridge flank	Upper ridge flank	Cone E of Ridge	Cone E of Ridge	Upper ridge flank	Upper ridge flank	Upper ridge flank
Latitude (S)	34.77	35.05	35.05	35.14	35.14	35.33	35.33	35.37
Longitude (E)	177.71	177.51	177.51	177.37	177.37	177.25	177.25	178.18
Water depth (mbsl)	1420-1270	1075-890	1075-890	1300-1315	1300-1315	1461-1269	1461-1269	1944-1780
Crystallinity	porphyritic	porphyritic	porphyritic	porphyritic	porphyritic	porphyritic	porphyritic	porphyritic
Major el ements (wt.%)								
SiO_2	49.60	48.15	47.16	46.56	45.77	54.07	52.86	45.35
TiO_2	0.83	1.05	1.09	0.76	0.78	0.73	0.74	0.95
Al_2O_3	19.50	18.50	19.32	19.92	20.34	16.99	17.05	19.62
$Fe_2O_3^t$	9.86	10.72	10.69	9.43	8.98	8.03	8.27	12.90
MnO	0.14	0.20	0.19	0.15	0.15	0.17	0.17	0.20
MgO	4.01	4.51	4.87	5.23	4.19	5.06	5.39	4.03
CaO	8.63	10.66	11.15	11.85	12.79	9.12	9.49	11.85
Na_2O	3.47	2.74	2.72	2.42	2.52	2.96	2.86	2.65
K_2O	1.10	0.57	0.39	0.32	0.27	1.37	1.20	0.19
P_2O_5	0.14	0.24	0.55	0.43	0.60	0.20	0.21	0.33
LOI	1.86	1.96	2.18	2.99	3.49	0.80	1.04	1.86
Original Total	99.19	99.35	100.34	100.09	99.89	99.59	99.32	99.92
Trace elements (ppm)								
Sc	29.2	37.8	39.4	32.9	30.4	28.6	30.4	43.0
V	300	-	362	303	317	231	229	-
Cr	22.0	34.0	35.0	87.0	57.0	95.0	106	15.0
Co	24.3	30.6	28.9	27.9	24.0	26.7	27.6	37.3
Ni	12.4	15.2	21.8	37.0	28.7	26.6	33.7	27.3
Cu	38.6	145	127	99.3	90.7	68.1	70.0	124
Zn	74.0	94.0	101	83.0	91.0	67.0	68.0	113
Ga	18.2	18.3	17.8	17.4	17.7	16.8	16.2	18.8
Mo	1.52	1.05	0.91	0.93	0.71	1.34	1.17	1.05
Sb	0.17	0.090	0.26	0.22	0.25	0.060	0.050	1.70
Sn	0.63	0.93	0.95	0.57	0.60	0.68	0.70	0.59
Cs	0.013	0.20	0.18	0.076	0.11	0.096	0.59	0.50
Tl	0.10	0026	0.009	0.025	0.005	0.065	0.055	0.17
Li	16.3	17.0	22.8	19.3	20.5	7.60	11.7	10.9
Rb	17.3	7.26	2.95	2.95	2.19	27.6	23.8	1.05
Sr	364	509	1477	610	575	428	512	445
Y	24.8	27.6	29.3	21.3	24.1	21.0	21.3	22.4
Zr	78.0	95.0	109	65.0	64.0	115	110	48.0
Nb	1.67	2.51	2.62	1.63	1.63	3.93	3.84	1.33
Ta	0.094	0.15	0.15	0.090	0.094	0.25	0.23	0.081
Ba	524	400	340	212	227	621	564	131
La	9.34	15.1	15.4	11.5	13.7	16.9	16.9	6.32
Ce	20.6	31.6	31.8	22.9	25.5	33.2	32.5	12.6
Pr	3.02	4.42	4.49	3.21	3.49	4.29	4.32	1.96
Nd	14.0	19.4	20.11	14.2	14.9	18.0	17.7	9.31
Sm	3.57	4.55	4.67	3.18	3.31	3.81	3.83	2.51
Eu	1.08	1.34	1.38	1.07	1.10	1.12	1.13	0.96
Gd	3.97	4.76	4.80	3.28	3.38	3.62	3.68	2.97
Tb	0.64	0.74	0.76	0.51	0.53	0.56	0.56	0.50
Dy	4.18	4.83	4.91	3.30	3.47	3.58	3.64	3.37
Ho	0.86	0.97	1.03	0.70	0.72	0.73	0.75	0.71
Er	2.57	2.95	3.01	2.08	2.17	2.17	2.18	2.16
Tm	0.37	0.42	0.44	0.30	0.32	0.31	0.32	0.32
Yb	2.48	2.74	2.88	1.99	2.14	2.15	2.18	2.09
Lu	0.37	0.42	0.43	0.31	0.34	0.33	0.34	0.32
Hf	2.15	2.84	2.98	1.72	1.73	2.82	2.81	1.37
Pb	2.50	3.80	3.80	2.80	3.00	3.30	3.30	1.70
Th	1.59	3.21	3.24	1.93	2.25	3.84	3.82	0.76
U	0.60	0.72	0.76	0.58	1.04	0.96	0.86	1.35

Table 1: Major and trace element composition of Colville Ridge lavas (continued)

Sample No.	TAN1313 DR11-1	TAN1313 DR11-3	TAN1313 DR12-1	TAN1512 DR06-1	TAN1512 DR06-2	TAN1512 DR06-3	TAN1512 DR11-1	TAN1512 DR11-2
Edifice	Colville Ridge	Colville Ridge	Colville Ridge	Colville Ridge	Colville Ridge	Colville Ridge	Colville Ridge	Colville Ridge
Location	Faulted cone	Faulted cone	Ridge-like cone	Upper ridge flank	Upper ridge flank	Upper ridge flank	Cone W of Ridge	Cone W of Ridge
Latitude (S)	35.59	35.59	35.64	32.81	32.81	32.81	33.66	33.66
Longitude (E)	177.21	177.21	176.99	178.23	177.37	178.23	178.02	178.02
Water depth (mbsl)	1882-1677	1882-1677	1400-1395	1748-1526	1748-1526	1748-1526	1768-1608	1768-1608
Crystallinity	aphyric	aphyric	porphyritic	aphyric	porphyritic	porphyritic	aphyric	aphyric
Major elements (wt%)								
SiO_2	48.28	45.60	49.31	51.71	44.55	56.56	45.08	48.03
TiO_2	1.10	1.10	0.82	0.97	0.83	0.77	1.64	1.63
Al_2O_3	18.44	18.49	17.71	16.67	19.89	18.04	20.38	21.06
$Fe_2O_3^t$	12.44	13.03	11.24	10.96	10.85	7.71	8.86	8.73
MnO	0.21	0.20	0.17	0.19	0.19	0.16	0.07	0.09
MgO	4.41	4.20	5.20	4.17	5.93	2.31	3.08	2.46
CaO	11.11	12.46	10.57	7.95	10.33	7.22	8.61	7.86
Na_2O	2.95	2.56	2.67	3.67	2.59	3.80	4.16	4.49
K_2O	0.27	0.16	0.58	0.95	0.29	1.32	1.1	1.27
P_2O_5	0.21	0.32	0.16	0.19	0.31	0.19	1.78	0.88
LOI	0.87	1.45	1.21	2.60	4.79	1.66	4.65	3.01
Original Total	100.29	99.59	99.66	100.08	100.57	99.75	99.47	99.58
Trace elements (ppm)								
Sc	39.5	43.6	36.1	31.8	31.6	21.1	25.5	19.6
V	-	-	304	327	325	136	201	196
Cr	16.0	14.0	39.0	3.00	30.0	4.00	198	156
Co	35.5	40.8	36.9	31.5	30.3	16.1	16.1	15.5
Ni	15.9	28.4	26.9	6.00	24.7	3.90	89.2	63.7
Cu	124	114	146	213	160	30.9	73.0	68.1
Zn	110	132	88.0	115	85.0	80.0	91.0	100
Ga	18.3	17.9	17.1	19.0	17.0	17.7	16.3	17.7
Mo	0.81	1.14	0.86	0.86	1.10	1.51	0.89	0.83
Sb	0.36	2.16	0.22	0.08	0.18	0.09	3.36	3.31
Sn	0.72	0.69	0.73	0.97	0.78	0.95	1.63	1.46
Cs	0.066	-	0.19	0.66	0.053	0.64	0.040	0.081
Tl	0.083	-	0.016	0.061	0.006	0.068	0.044	0.090
Li	10.0	9.50	12.2	21.8	25.6	10.3	15.5	13.4
Rb	2.58	1.19	6.24	13.9	2.34	22.8	12.9	20.6
Sr	438	444	334	385	715	348	916	564
Y	23.1	32.5	21.1	29.0	21.4	26.6	64.8	35.5
Zr	58.0	58.0	69.0	102	67.0	127	160	188
Nb	2.14	1.87	1.75	1.70	1.21	2.03	30.0	30.1
Ta	0.14	0.13	0.11	0.11	0.079	0.13	1.85	1.86
Ba	180	123	328	550	204	558	283	290
La	7.80	7.59	7.99	11.2	7.46	8.97	29.9	21.6
Ce	17.1	13.4	17.2	24.4	16.6	19.9	39.1	38.3
Pr	2.55	2.16	2.49	3.73	2.44	2.95	6.30	5.01
Nd	12.1	10.5	11.3	17.5	11.7	13.7	26.7	21.0
Sm	3.12	2.93	2.93	4.44	3.06	3.61	5.31	4.33
Eu	1.14	1.09	0.93	1.42	0.99	1.08	1.84	1.52
Gd	3.61	3.53	3.24	5.01	3.52	4.15	5.87	4.57
Tb	0.59	0.57	0.53	0.79	0.55	0.67	0.91	0.70
Dy	3.85	3.85	3.48	5.19	3.70	4.36	6.27	4.64
Ho	0.80	0.86	0.74	1.08	0.78	0.92	1.39	0.98
Er	2.40	2.72	2.18	3.19	2.26	2.81	4.50	3.00
Tm	0.34	0.39	0.31	0.47	0.34	0.41	0.64	0.43
Yb	12.23	2.62	2.09	3.02	2.19	2.71	4.24	2.74
Lu	0.34	0.43	0.32	0.46	0.33	0.42	0.69	0.42
Hf	1.73	1.52	2.02	2.97	2.11	3.60	3.78	4.12
Pb	2.10	1.90	3.30	4.70	2.80	4.20	2.50	2.60
Th	1.06	0.62	1.91	1.65	1.60	2.10	2.88	2.83
U	0.29	0.76	0.33	0.46	0.97	0.63	4.63	3.41

Table 1: Major and trace element composition of Colville Ridge lavas (continued)

Sample No.	TAN1512 DR13-1	TAN1512 DR13-2	TAN1512 DR14-1	TAN1512 DR15-1	TAN1512 DR16-1	TAN1512 DR19-1	TAN1512 DR19-2	TAN1512 DR22-1
Edifice	Colville Ridge	Colville Ridge	Colville Ridge	Colville Ridge	Colville Ridge	Colville Ridge	Colville Ridge	Colville Ridge
Location	Upper ridge flank	Upper ridge flank	Upper ridge flank	Upper ridge flank	Upper ridge flank	Upper ridge flank	Upper ridge flank	Upper ridge flank
Latitude (S)	33.71	33.71	33.78	33.89	33.89	34.00	34.00	34.37
Longitude (E)	178.24	178.24	178.25	178.16	178.16	178.10	178.10	177.88
Water depth (mbsl)	1660-1384	1660-1384	1100-974	1150-1080	1170-1084	1049-1035	1049-1035	1440-1379
Crystallinity	aphyric	aphyric	porphyritic	aphyric	porphyritic	porphyritic	porphyritic	porphyritic
Major elements (wt%)								
SiO_2	44.66	44.68	55.43	43.95	54.43	56.68	55.26	48.06
TiO_2	0.65	0.67	0.96	1.24	0.69	0.61	0.61	0.74
Al_2O_3	17.71	17.83	17.84	17.05	16.65	17.26	17.62	17.58
$Fe_2O_3^t$	11.45	11.53	8.82	15.66	9.57	7.56	7.61	11.62
MnO	0.21	0.23	0.22	0.22	0.18	0.14	0.14	0.20
MgO	7.62	7.45	2.54	4.62	4.60	3.25	3.48	4.81
CaO	13.18	13.00	5.92	9.69	8.61	8.17	8.61	11.62
Na_2O	1.75	1.80	4.56	2.73	2.84	3.05	3.06	2.35
K_2O	0.20	0.22	2.26	0.29	1.17	1.65	1.35	0.66
P_2O_5	0.40	0.38	0.42	0.64	0.12	0.18	0.24	0.15
LOI	1.79	1.95	0.48	3.38	0.91	1.07	1.29	0.68
Original Total	99.68	99.78	99.52	99.51	99.82	99.71	99.30	99.93
Trace elements (ppm)								
Sc	49.9	48.9	23.6	49.0	32.0	22.1	22.7	n.a.
V	317	325	78.7	adl	258	167	168	n.a.
Cr	282	275	3.00	8.00	23.0	53.0	69.0	n.a.
Co	44.0	44.8	12.9	32.9	29.3	20.7	21.6	n.a.
Ni	79.0	83.2	4.30	29.1	16.3	12.0	15.5	n.a.
Cu	56.8	70.8	5.50	214	123	67.9	71.5	n.a.
Zn	80.0	91.0	118	136	73.0	66.0	67.0	n.a.
Ga	14.0	14.2	19.3	17.5	15.7	16.3	16.3	n.a.
Mo	0.57	1.29	0.83	0.82	1.32	1.57	1.49	n.a.
Sb	0.61	0.69	0.20	0.89	0.08	0.10	0.10	n.a.
Sn	0.53	0.55	1.29	0.97	0.72	0.96	0.96	n.a.
Cs	0.014	0.016	0.25	bdl	0.65	1.42	1.03	n.a.
Tl	0.091	0.12	0.039	0.019	0.048	0.069	0.060	n.a.
Li	7.70	8.50	12.1	23.1	12.7	9.00	13.0	n.a.
Rb	1.20	1.38	35.03	1.06	20.0	32.4	26.0	n.a.
Sr	331	330	318	831	398	414	747	n.a.
Y	17.4	20.5	39.1	32.8	23.3	23.6	22.9	n.a.
Zr	29.0	34.0	148	88.0	90.0	108	106	n.a.
Nb	0.83	0.89	2.86	1.94	2.25	2.29	2.33	n.a.
Ta	0.051	0.051	0.18	0.12	0.14	0.15	0.15	n.a.
Ba	152	154	750	345	427	596	536	n.a.
La	4.19	5.14	13.3	8.53	10.1	9.90	9.96	n.a.
Ce	8.18	8.02	29.84	18.92	21.7	21.7	21.3	n.a.
Pr	1.37	1.51	4.43	2.96	3.05	3.03	2.99	n.a.
Nd	6.81	7.65	21.0	15.0	13.6	13.4	13.4	n.a.
Sm	1.87	2.11	5.50	4.11	3.36	3.35	3.32	n.a.
Eu	1.63	1.84	4.12	3.44	2.42	2.49	2.46	n.a.
Gd	2.31	2.55	6.32	4.98	3.59	3.68	3.07	n.a.
Tb	0.34	0.40	0.98	0.79	.058	0.59	0.59	n.a.
Dy	2.41	2.84	6.56	5.25	3.85	3.92	3.92	n.a.
Ho	0.53	0.60	1.38	1.11	0.81	0.82	0.82	n.a.
Er	1.63	1.84	4.12	3.44	2.42	2.49	2.46	n.a.
Tm	0.23	0.26	0.60	0.49	0.36	0.37	0.36	n.a.
Yb	1.50	1.75	3.93	3.17	2.38	2.38	2.34	n.a.
Lu	0.23	0.28	0.60	0.50	0.38	0.38	0.37	n.a.
Hf	0.94	1.08	4.31	2.68	2.58	3.18	3.21	n.a.
Pb	1.60	2.30	5.30	4.30	3.60	4.90	5.00	n.a.
Th	0.53	0.55	2.81	1.48	2.90	3.36	3.31	n.a.
U	2.73	3.38	1.30	2.61	0.75	0.96	0.90	n.a.

Table 1: Major and trace element composition of Colville and Kermadec Ridge lavas (continued)

Sample No.	TAN1512 DR22-2	TAN1213 DR64-2	TAN1213 DR64-12	SO255 DR30-2	SO255 DR30-4	SO255 DR31-1	SO255 DR31-3	SO255 DR32-1
Edifice	Colville Ridge	Kermadec Ridge	Kermadec Ridge	Kermadec Ridge	Kermadec Ridge	Kermadec Ridge	Kermadec Ridge	Kermadec Ridge
Location	Upper ridge flank	Upper ridge flank	Upper ridge flank	NW facing cliff	NW facing cliff	SW facing cliff	SW facing cliff	NW facing scarp
Latitude (S)	34.37	36.13	36.13	34.55	34.55	34.49	34.49	34.25
Longitude (E)	177.88	178.43	178.43	179.48	179.48	179.48	179.48	179.51
Water depth (mbsl)	1440-1379	2120-1810	2120-1810	2235-1720	2235-1720	2670-2330	2670-2330	2990-2537
Crystallinity	porphyritic	aphyric	porphyritic	porphyritic	porphyritic	porphyritic	porphyritic	porphyritic
Major elements (wt%)								
SiO_2	50.49	55.79	54.12	54.98	56.33	51.64	51.43	52.42
TiO_2	0.74	1.01	0.83	0.71	0.69	0.76	0.70	0.72
Al_2O_3	19.33	15.93	17.29	16.65	15.79	18.11	16.58	16.39
$Fe_2O_3^t$	10.05	10.56	9.84	8.37	9.08	10.03	9.98	9.26
MnO	0.17	0.19	0.16	0.16	0.17	0.16	0.17	0.15
MgO	3.62	3.01	3.25	3.50	3.81	3.88	5.54	5.19
CaO	10.53	6.94	8.42	8.55	8.31	9.91	10.98	10.52
Na_2O	2.63	3.60	3.12	2.94	2.99	2.68	2.34	2.46
K_2O	0.61	1.39	0.92	0.99	0.92	0.63	0.65	0.78
P_2O_5	0.11	0.25	0.15	0.44	0.19	0.12	0.19	0.15
LOI	0.91	1.21	1.97	1.93	0.78	1.39	0.75	1.41
Original Total	99.32	99.95	100.07	99.37	99.20	99.44	99.46	99.59
Trace elements (ppm)								
Sc	33.0	31.5	26.9	29.5	33.9	27.9	43.6	42.8
V	adl	247	309	267	289	337	378	351
Cr	11.0	bdl	7.00	16.3	30.6	33.1	149	136
Co	33.2	25.8	24.5	22.7	30.1	19.2	37.3	35.5
Ni	13.0	4.80	7.60	7.85	13.1	16.1	32.9	32.6
Cu	75.9	77.1	48.0	80.4	72.2	150	131	140
Zn	85.0	104	88.0	89.5	84.6	80.3	82.1	77.5
Ga	17.7	17.6	17.3	16.8	16.3	17.7	16.6	16.6
Mo	0.54	1.06	0.61	-	-	-	-	-
Sb	0.10	0.09	0.05	-	-	-	-	-
Sn	0.51	1.26	0.080	-	-	-	-	-
Cs	0.077	0.85	0.087	0.49	0.53	0.34	0.32	0.72
Tl	0.006	0.159	0.034	--	-	-	-	-
Li	9.10	7.60	17.2	7.88	8.79	11.8	6.29	11.9
Rb	5.12	20.13	9.94	15.5	15.5	10.4	9.94	18.2
Sr	305	310	281	275	245	343	321	320
Y	16.4	34.6	24.7	38.5	24.9	19.2	18.5	19.3
Zr	37.0	115	88.0	74.0	81.3	53.1	54.3	60.1
Nb	0.62	2.60	1.95	1.34	1.20	0.90	0.82	0.87
Ta	0.037	0.16	0.12	0.097	0.081	0.063	0.053	0.058
Ba	277	569	419	386	455	347	320	322
La	4.30	14.9	9.75	5.31	5.51	3.66	3.35	6.32
Ce	9.35	31.2	20.6	12.7	12.6	8.87	7.95	15.0
Pr	1.38	4.45	2.98	1.97	1.92	1.42	1.27	2.17
Nd	6.99	19.5	13.3	9.91	9.43	7.22	6.60	10.5
Sm	1.96	4.90	3.34	2.93	2.74	2.22	2.05	2.82
Eu	0.73	1.43	1.04	0.99	0.90	0.82	0.75	0.95
Gd	2.47	5.45	3.80	3.79	3.25	2.72	2.51	3.06
Tb	0.41	0.86	0.62	0.67	0.57	0.47	0.44	0.50
Dy	2.78	5.62	4.01	4.73	3.84	3.12	2.92	3.16
Ho	0.59	1.21	0.85	1.10	0.84	0.67	0.62	0.66
Er	1.84	3.62	2.54	3.18	2.57	1.82	1.87	1.98
Tm	0.26	0.53	0.38	0.52	0.38	0.29	0.27	0.28
Yb	1.71	3.53	2.51	3.55	2.57	1.94	1.83	1.92
Lu	0.27	0.55	0.33	0.59	0.41	0.31	0.29	0.30
Hf	1.16	3.35	2.47	1.91	1.98	1.41	1.35	1.47
Pb	3.00	5.20	2.80	2.97	2.94	2.98	2.61	2.89
Th	0.77	3.58	2.50	0.72	0.86	0.52	0.47	1.11
U	0.27	0.87	0.75	1.91	1.51	0.19	0.19	0.80

Table 1: Major and trace element composition of Kermadec Ridge lavas (continued)

Sample No.	SO255 DR32-8	SO255 DR35-2	SO255 DR35-4	SO255 DR35-6	SO255 DR35-9	SO255 DR139-2	SO255 DR139-8	SO255 DR139-12
Edifice	Kermadec Ridge	Kermadec Ridge	Kermadec Ridge	Kermadec Ridge	Kermadec Ridge	Kermadec Ridge	Kermadec Ridge	Kermadec Ridge
Location	NW facing scarp	NW scarp upper part	NW scarp upper part	NW scarp upper part	NW facing cliff	SW facing slope	SW facing slope	NW facing slope
Latitude (S)	34.25	34.35	34.35	34.35	34.35	32.93	32.93	32.93
Longitude (E)	179.48	179.61	179.61	179.61	179.61	180.47	180.47	180.47
Water depth (mbsl)	2990-2537	1739-1459	1739-1459	1739-1459	1739-1459	995-633	995-633	995-633
Crystallinity	porphyritic	porphyritic	porphyritic	porphyritic	porphyritic	porphyritic	porphyritic	porphyritic
Major elements (wt%)								
SiO_2	50.48	49.02	49.16	49.20	65.75	47.76	48.80	48.97
TiO_2	0.81	1.07	1.09	1.09	0.65	0.56	0.87	0.82
Al_2O_3	18.40	18.50	18.72	18.51	14.87	20.11	18.35	18.16
$Fe_2O_3^t$	9.70	11.79	11.89	11.86	5.28	9.77	10.99	10.60
MnO	0.14	0.23	0.25	0.25	0.10	0.15	0.19	0.19
MgO	3.86	3.57	3.60	3.60	1.18	5.06	4.40	4.47
CaO	10.55	7.22	7.42	7.31	3.24	13.21	9.25	9.27
Na_2O	2.51	4.61	4.23	4.27	4.75	1.94	3.26	3.41
K_2O	0.58	0.71	1.01	1.05	2.01	0.30	0.94	0.71
P_2O_5	0.13	0.22	0.22	0.23	0.19	0.04	0.50	0.27
LOI	1.93	2.06	2.12	2.02	1.28	0.94	1.48	2.25
Original Total	99.22	99.19	99.90	99.59	99.46	100.00	99.34	99.27
Trace elements (ppm)								
Sc	31.5	37.4	37.9	36.6	16.3	41.1	40.1	38.1
V	347	369	385	367	62.5	316	337	295
Cr	23.1	1..9	14.2	14.1	4.79	21.4	28.3	23.3
Co	29.7	28.3	28.3	28.6	7.16	38.0	33.4	30.9
Ni	18.8	9.97	10.7	11.0	1.75	18.1	38.6	20.8
Cu	160	145	105	143	18.5	107	92.7	66.9
Zn	76.6	102	106	104	80.7	67.8	105	86.0
Ga	17.85	21.9	22.6	21.7	17.3	17.0	17.9	17.0
Mo	-	-	-	-	-	-	-	-
Sb	-	-	-	-	-	-	-	-
Sn	-	-	-	-	-	-	-	-
Cs	0.59	0.41	0.34	0.35	0.63	1.10	0.050	0.042
Tl	-	-	-	-	-	-	-	-
Li	14.7	17.2	17.5	17.2	30.4	15.0	19.7	9.94
Rb	11.3	7.96	12.4	13.0	37.3	10.1	5.34	7.73
Sr	318	449	443	440	257	357	1011	303
Y	19.4	32.0	31.1	30.1	37.9	12.9	33.4	29.6
Zr	47.7	90.0	91.7	90.4	150	27.8	95.8	75.3
Nb	0.77	1.40	1.43	1.40	2.35	0.27	1.71	1.01
Ta	0.055	0.092	0.094	0.094	0.152	0.026	0.099	0.074
Ba	322	481	641	630	920	114	775	282
La	6.09	11.7	11.7	11.5	15.0	1.50	14.5	6.29
Ce	13.4	25.2	25.2	24.9	33.5	3.40	30.4	14.5
Pr	1.97	3.81	3.88	3.83	4.77	0.71	4.39	2.32
Nd	3.52	18.01	18.5	18.1	22.0	4.02	20.5	11.6
Sm	2.66	4.79	4.87	4.82	5.63	1.41	4.99	3.46
Eu	0.93	1.56	1.59	1.55	1.58	0.60	1.48	1.16
Gd	3.01	5.19	5.29	5.24	6.01	1.81	5.12	4.12
Tb	0.50	0.84	0.85	0.84	0.98	0.33	0.82	0.72
Dy	3.23	5.35	5.34	5.30	6.23	2.20	5.11	4.75
Ho	0.68	1.10	1.11	1.09	1.30	0.47	1.07	1.02
Er	1.83	2.96	2.91	2.84	3.52	1.39	3.19	2.77
Tm	0.29	0.47	0.45	0.44	0.57	0.20	0.45	0.45
Yb	1.97	3.08	2.91	2.83	3.83	1.34	3.03	2.98
Lu	0.31	0.47	0.44	0.43	0.60	0.21	0.48	0.47
Hf	1.32	2.43	2.49	2.44	4.01	0.79	2.61	2.18
Pb	3.49	4.74	4.30	3.96	5.76	1.40	5.91	3.69
Th	1.13	1.59	1.62	1.60	2.93	0.12	2.21	0.83
U	0.79	0.69	0.71	0.71	0.91	0.11	1.49	0.99

Table 1: Major and trace element composition of Kermadec Ridge lavas (continued)

Sample No.	SO255 DR139-15	SO255 DR139-16	SO255 DR139-17	SO255 DR178-2	SO255 DR178-3	SO255 DR179-1	SO255 DR179-5	SO255 DR179-8
Edifice	Kermadec Ridge	Kermadec Ridge	Kermadec Ridge	Kermadec Ridge	Kermadec Ridge	Kermadec Ridge	Kermadec Ridge	Kermadec Ridge
Location	NW facing slope	NW scarp slope	NW scarp upper part	Cone-like structure	Cone-like structure	NW facing slope	NW facing slope	NW facing slope
Latitude (S)	32.93	32.93	34.35	34.17	34.17	34.22	34.22	34.22
Longitude (E)	180.47	180.47	180.47	179.76	179.76	179.71	179.71	179.71
Water depth (mbsl)	995-633	995-633	995-633	1200-838	1200-838	1106-738	1106-738	1106-738
Crystallinity	porphyritic	porphyritic	porphyritic	porphyritic	porphyritic	porphyritic	porphyritic	porphyritic
Major elements (wt%)								
SiO_2	53.67	50.13	55.74	49.29	42.55	47.21	47.20	48.90
TiO_2	1.11	1.22	0.84	0.81	0.80	0.84	0.69	0.91
Al_2O_3	14.95	15.86	18.31	19.12	17.38	17.99	18.39	18.01
$Fe_2O_3^t$	12.44	12.48	7.98	11.18	11.72	11.29	11.49	11.84
MnO	0.39	0.57	0.26	0.19	0.48	0.19	0.16	0.18
MgO	3.61	4.50	1.08	3.63	3.18	3.97	4.89	4.49
CaO	6.43	6.03	3.73	11.05	13.88	12.27	12.15	10.78
Na_2O	3.99	3.39	6.07	2.65	2.78	2.31	2.01	2.72
K_2O	1.10	0.79	2.03	0.44	0.71	0.50	0.46	0.52
P_2O_5	0.22	0.18	0.28	0.09	0.24	0.11	0.05	0.10
LOI	1.16	5.16	2.56	0.78	5.70	2.49	1.50	0.51
Original Total	99.27	99.95	99.06	99.35	99.31	99.31	99.12	99.12
Trace elements (ppm)								
Sc	29.4	36.3	19.0	35.8	38.8	43.9	45.3	49.3
V	309	457	27.8	363	378	415	311	416
Cr	4.94	5.43	5.33	11.5	12.1	24.6	40.5	32.5
Co	31.4	27.5	10.8	32.5	34.2	43.0	39.8	37.6
Ni	18.5	36.5	21.5	10.7	27.3	19.0	21.0	15.2
Cu	188	220	36.9	159	150	137	192	168
Zn	130	185	111	85.5	812	83.8	66.7	95.3
Ga	23.8	19.9	21.0	18.4	17.4	17.9	16.9	19.3
Mo	-	-	-	-	-	-	-	-
Sb	-	-	-	-	-	-	-	-
Sn	-	-	-	-	-	-	-	-
Cs	6.09	0.12	0.12	0.30	0.070	0.21	0.069	0.089
Tl	-	-	-	-	-	-	-	-
Li	11.0	42.7	10.3	8.36	11.1	9.35	7.59	7.31
Rb	45.5	1.70	15.3	7.05	6.77	5.10	3.86	3.67
Sr	342	323	312	423	417	388	368	355
Y	37.0	30.2	40.4	18.6	21.4	19.2	13.5	21.9
Zr	82.4	73.6	159	41.0	41.6	45.7	30.9	56.3
Nb	1.16	0.95	2.61	0.66	0.65	0.82	0.45	1.00
Ta	0.079	0.069	0.18	0.049	0.048	0.059	0.036	0.066
Ba	841	280	977	242	302	337	176	324
La	9.55	6.08	12.37	3.88	418	5.52	2.42	5.31
Ce	20.8	14.1	37.4	9.12	8.48	12.3	6.09	12.3
Pr	3.42	2.35	4.61	1.46	1.46	1.91	0.98	1.92
Nd	17.0	12.0	22.5	7.47	7.54	9.32	5.21	9.56
Sm	4.79	3.67	6.29	2.27	2.27	2.65	1.71	2.84
Eu	1.57	1.45	2.13	0.91	0.90	0.95	0.72	1.03
Gd	5.44	4.34	6.84	2.74	2.80	3.07	2.03	3.31
Tb	0.91	0.75	1.12	0.47	0.48	0.50	0.35	0.57
Dy	5.86	4.94	7.05	3.07	3.25	3.26	2.32	3.68
Ho	1.23	1.04	1.44	0.66	0.70	0.68	0.48	0.77
Er	3.31	2.82	3.81	1.77	1.90	1.82	1.29	2.30
Tm	0.53	0.45	0.60	0.28	0.31	0.29	0.21	0.33
Yb	3.47	2.99	3.96	1.87	2.06	1.86	1.36	2.17
Lu	0.54	0.47	0.63	0.30	0.33	0.29	0.21	0.34
Hf	2.34	2.03	5.39	1.17	1.14	1.31	0.91	1.52
Pb	6.97	3.39	7.29	2.00	2.25	2.04	1.81	2.02
Th	1.19	0.65	2.43	0.35	0.33	0.78	0.38	0.70
U	0.57	0.37	0.89	0.27	1.07	0.15	0.25	0.17

Table 1: Major and trace element composition of Kermadec Ridge lavas (continued)

Sample No.	SO255 DR179-12	SO255 DR179-14	SO255 DR179-15	SO255 DR179-16	SO255 DR179-17
Edifice	Kermadec Ridge	Kermadec Ridge	Kermadec Ridge	Kermadec Ridge	Kermadec Ridge
Location	NW facing slope	NW facing slope	NW facing slope	NW facing slope	NW facing slope
Latitude (S)	34.22	34.22	34.22	34.22	34.22
Longitude (E)	179.76	179.71	179.71	179.71	179.71
Water depth (mbsl)	1106-738	1106-738	1106-738	1106-738	1106-738
Crystallinity	porphyritic	porphyritic	porphyritic	porphyritic	porphyritic
Major elements (wt%)					
SiO_2	51.23	49.47	59.95	49.57	50.74
TiO_2	0.88	0.99	0.79	0.99	0.96
Al_2O_3	19.11	17.24	16.04	17.14	16.34
$Fe_2O_3^t$	9.17	11.85	7.18	11.89	12.12
MnO	0.16	0.19	0.20	0.21	0.21
MgO	3.18	4.57	1.70	4.55	4.78
CaO	10.11	10.40	4.68	10.49	9.99
Na_2O	3.20	2.88	4.38	2.87	2.81
K_2O	0.97	0.42	1.77	0.46	0.47
P_2O_5	0.18	0.20	0.31	0.19	0.14
LOI	0.94	0.75	2.25	0.61	0.38
Original Total	99.16	99.10	99.43	99.12	99.07
Trace elements (ppm)					
Sc	38.1	46.4	25.9	46.3	43.1
V	350	428	50.4	424	399
Cr	13.4	19.1	5.71	19.31	17.9
Co	28.2	34.3	11.6	37.5	37.5
Ni	7.66	11.6	4.86	11.7	10.7
Cu	87.7	103	22.7	170	151
Zn	92.4	98.2	138	136	101
Ga	19.5	19.0	18.9	19.2	18.0
Mo	-	-	-	-	-
Sb	-	-	-	-	-
Sn	-	-	-	-	-
Cs	0.11	0.14	0.73	0.082	0.22
Tl	-	-	-	-	-
Li	9.33	6.94	12.7	8.52	5.40
Rb	7.61	4.06	33.1	3.52	6.44
Sr	388	343	344	342	323
Y	28.4	24.0	46.8	24.6	23.3
Zr	89.5	53.3	194	53.8	52.1
Nb	1.44	1.10	3.52	1.13	1.07
Ta	0.10	0.075	0.21	0.076	0.072
Ba	469	257	938	284	289
La	7.77	5.78	17.4	5.96	5.69
Ce	17.8	13.5	40.3	14.0	13.2
Pr	2.62	2.13	5.71	2.17	2.06
Nd	12.6	10.7	26.5	11.0	10.3
Sm	3.56	3.17	6.90	3.23	3.04
Eu	1.13	1.14	1.89	1.16	1.08
Gd	4.12	3.71	7.34	3.78	3.60
Tb	0.70	0.62	1.22	0.64	0.60
Dy	4.59	4.09	7.75	4.15	3.93
Ho	0.98	0.85	1.62	0.88	0.83
Er	2.66	2.27	4.85	2.33	2.23
Tm	0.43	0.36	0.70	0.37	0.35
Yb	2.88	2.38	4.67	2.48	2.35
Lu	0.46	0.37	0.73	0.39	0.37
Hf	2.40	1.53	4.95	1.53	1.48
Pb	3.43	2.45	7.58	2.75	2.53
Th	1.56	0.65	3.62	0.66	0.62
U	0.78	0.21	0.93	0.19	0.17

adl = above detection limit; bdl = below detection limit; n.a. = not analysed; TAN samples have been analysed at OGL, Ontario, Canada; SO255 samples have been analysed at the University of Hamburg (XRF) and University of Kiel (ICPMS).

Table 2

Table 2. $^{40}Ar/^{39}Ar$ step-heating results from the Colville and Kermadec Ridges.

Sample #	Location	Material	Lab. ID #	Plateau age ± 2σ (Ma)	MSWD	P %	% ^{39}Ar	Steps	Inverse isochron age ± 2σ (Ma)	$(^{40}Ar/^{36}Ar)_i$ ± 2σ	MSWD	P %	SF %	Steps	Steps with fresh material[a]	Wt.% K[b]	Comments
TAN1313 DR11-1	Colville Ridge	Plagioclase	11-1f	7.5 ± 2.0	1.57	14	70.9	8-15	6.9 ± 1.6	*303.3 ± 6.3*	0.77	60	85.1	8-15	5-8, 10-15	0.02	
TAN1512 DR16-1	Colville Ridge	Plagioclase	16-1f	2.63 ± 0.23	1.21	25	100.0	1-16	2.29 ± 0.61	311 ± 34	1.22	25	*22.2*	1-16	None	0.12	
TAN1512 DR19-2	Colville Ridge	Plagioclase	19-2f	3.80 ± 0.33	1.57	17	66.1	7-12	4.2 ± 1.2	280 ± 52	1.81	12	*19.1*	7-12	None	0.11	
TAN1213 DR 64-1	Kermadec Ridge	Plagioclase	64-1f	3.40 ± 0.24	1.04	40	63.5	7-15	3.82 ± 0.61	276 ± 29	1.04	40	40.2	7-15	None	0.11	High-T plateau
TAN1213 DR 64-1	Kermadec Ridge	Plagioclase	64-1f	3.06 ± 0.25	0.79	60	65.2	1-8	3.10 ± 0.34	294.2 ± 7.0	0.9	50	*26.6*	1-8	None	0.11	Low-T plateau
SO255 DR30-4	Kermadec Ridge	Groundmass	30-4m/1	4.44 ± 0.36	0.33	99	56.6	6-19	4.48 ± 0.34	276 ± 32	*0.25*	100	87.1	6-19	5-17	0.74	Split 1
SO255 DR30-4	Kermadec Ridge	Groundmass	30-4m/2	4.04 ± 1.23*	0.40	88	42.0	4-10	3.8 ± 1.6	300 ± 29	0.46	81	68.9	4-10	5-8	0.70	Split 2
SO255 DR30-4	Kermadec Ridge	Groundmass	30-4 m/(1+2)	4.41 ± 0.35	0.35	100											Combined age
SO255 DR139-2	Kermadec Ridge	Groundmass	1392m	4.6 ± 1.6	0.96	46	56.6	3-10	5.9 ± 2.4	266 ± 65	1.00	42	45.2	3-10	5-9	0.19	
SO255 DR179-5	Kermadec Ridge	Groundmass	1795m	4.8 ± 1.2	0.68	69	69.7	3-10	1.9 ± 2.0	395 ± 167	0.37	90	*16.9*	3-10	3-6	0.22	

Lab. ID # = Laboratory Identification number, MSWD = Mean Square Weighted Deviation, P = probability, SF = spreading factor, $(^{40}Ar/^{36}Ar)_i$ = initial $^{40}Ar/^{36}Ar$, Wt.% = weight %, and T = temperature.

*Pseudo-plateau (40-49% ^{39}Ar) age.

Values in italics indicate statistically invalid values (i.e., SF = < 40%, MSWD = < 0.30, or $(^{40}Ar/^{36}Ar)_i$ values are > or < 295.5).

[a]Steps numbers associated with the degassing of fresh material are determined from the $^{36}Ar/^{37}Ar$ plagioclase and $^{36}Ar/^{39}Ar$ basalt groundmass Alteration Index basaltic values (Baski, 2007; Supplementary Tables).

[b]Weight % K values are calculated from the combined $^{39}Ar_K$ values for each weighed sample.

Table 3

Table 3: Sr - Nd - Pb isotope ratios of the Colville and Kermadec Ridge lavas

Sample ID	Unit	Rock-type	$^{87}Sr/^{86}Sr$	$^{143}Nd/^{144}Nd$	$^{206}Pb/^{204}Pb$	$^{207}Pb/^{204}Pb$	$^{208}Pb/^{204}Pb$
TAN1313 DR03-1	Colville Ridge	Basalt	0.704379	0.512929	18.706	15.572	38.607
TAN1313 DR05-1A	Colville Ridge	Basalt	0.704243	0.512891	18.740	15.576	38.590
TAN1313 DR05-1C	Colville Ridge	Basalt	0.707089	0.512897	18.704	15.577	38.580
TAN1313 DR06-1	Colville Ridge	Basalt	0.704181	0.512886	18.685	15.550	38.492
TAN1313 DR06-3	Colville Ridge	Basalt	0.704171	0.512899	18.716	15.570	38.581
TAN1313 DR08-1	Colville Ridge	Basaltic andesite	0.704127	0.512889	18.744	15.562	38.551
TAN1313 DR08-3	Colville Ridge	Basalt	0.704115	0.512909	18.764	15.589	38.634
TAN1313 DR09-1	Colville Ridge	Basalt	0.704058	0.512916	18.721	15.571	38.572
TAN1313 DR11-1	Colville Ridge	Basalt	0.704069	0.512925	18.622	15.554	38.472
TAN1313 DR11-3	Colville Ridge	Basalt	0.703963	0.512952	18.718	15.583	38.607
TAN1313 DR12-1	Colville Ridge	Basalt	0.704289	0.512907	18.739	15.562	38.534
TAN1512 DR06-1	Colville Ridge	Basalt	0.704348	0.512955	18.615	15.567	38.564
TAN1512 DR06-2	Colville Ridge	(Picro-) Basalt	0.704413	0.512975	18.615	15.564	38.553
TAN1512 DR06-3	Colville Ridge	Basaltic andesite	0.704409	0.512960	18.653	15.584	38.596
TAN1512 DR11-1	Colville Ridge	Basalt	0.703126	0.512986	19.013	15.580	38.660
TAN1512 DR11-2	Colville Ridge	Basalt	0.703047	0.513011	18.990	15.565	38.637
TAN1512 DR14-1	Colville Ridge	Basaltic andesite	0.704436	0.512962	18.709	15.592	38.620
TAN1512 DR15-1	Colville Ridge	(Picro-) Basalt	0.704446	0.512957	18.715	15.622	38.768
TAN1512 DR16-1	Colville Ridge	Basaltic andesite	0.704285	0.512955	18.734	15.592	38.672
TAN1512 DR19-1	Colville Ridge	Basaltic andesite	0.704440	0.512937	18.739	15.600	38.660
TAN1512 DR22-2	Colville Ridge	Basalt	0.704489	0.512924	18.742	15.604	38.711
TAN1213 DR64-2	Kermadec Ridge	Basaltic andesite	0.704351	0.512927	18.793	15.612	38.694
TAN1213 DR64-12	Kermadec Ridge	Basaltic andesite	0.704337	0.512937	18.776	15.608	38.671
SO255 DR30-2	Kermadec Ridge	Basaltic andesite	0.704000	0.513005	18.677	15.578	38.600
SO255 DR30-4	Kermadec Ridge	Basaltic andesite	0.704056	0.512995	18.683	15.581	38.606
SO255 DR31-1	Kermadec Ridge	Basaltic andesite	0.704119	0.513003	18.683	15.579	38.649
SO255 DR31-3	Kermadec Ridge	Basaltic andesite	0.704137	0.512995	18.683	15.578	38.649
SO255 DR32-1	Kermadec Ridge	Basaltic andesite	0.703946	0.512950	18.802	15.616	38.650
SO255 DR32-8	Kermadec Ridge	Basaltic andesite	0.704031	0.512946	18.830	15.620	38.681
SO255 DR35-6	Kermadec Ridge	Basaltic andesite	0.704328	0.512946	18.637	15.575	38.554
SO255 DR35-9	Kermadec Ridge	Basaltic andesite	0.704389	0.512950	18.658	15.583	38.586
SO255 DR178-2	Kermadec Ridge	Basaltic andesite	0.704278	0.512976	18.651	15.569	38.578
SO255 DR179-5	Kermadec Ridge	Basaltic andesite	0.704299	0.512949	18.554	15.559	38.519
SO255 DR179-8	Kermadec Ridge	Basaltic andesite	0.704270	0.512958	18.618	15.564	38.545
SO255 DR179-12	Kermadec Ridge	Basaltic andesite	0.704248	0.512979	18.652	15.576	38.586
SO255 DR179-15	Kermadec Ridge	Basaltic andesite	0.704296	0.512956	18.632	15.569	38.565
SO255 DR179-17	Kermadec Ridge	Basaltic andesite	0.704265	0.512972	18.623	15.572	38.566

Supplementary File 1

Click here to download e-component: Supplementary_File_1_Majors_Traces_StandardData_REV.xlsx

Supplementary File 2

Click here to download e-component: SupplementaryFile2_ArAr_Analytical_Details.docx

Supplementary File 3

Click here to download e-component: Supplementary File 3.xlsx

Supplementary File 4

Click here to download e-component: Supplementary File_4_Modeling_Details.docx